Global and Planetary Change 202 (2021) 103501

Contents lists available at ScienceDirect

Global and Planetary Change

journal homepage: www.elsevier.com/locate/gloplacha

Dynamic interactions between subduction zones

Ágnes Király [a,*], Francesca Funiciello [b], Fabio A. Capitanio [c], Claudio Faccenna [b,d]

[a] Centre for Earth Evolution and Dynamics, University of Oslo, Norway
[b] Laboratory of Experimental Tectonics, Department of Sciences, University of Roma Tre, Italy
[c] School of Earth, Atmosphere and Environment, Monash University, Clayton, VIC, Australia
[d] Department of Geological Sciences, Jackson School of Geosciences, University of Texas at Austin, USA

ARTICLE INFO

Keywords:
Subduction dynamics
Slab-slab interaction
Mediterranean
Analog modeling
Mantle flow

ABSTRACT

A common feature of tectonic reconstructions is the migration of subduction zones and their interactions, resulting in complex tectonic patterns. Reduced migration rates, uplift, strong rotations, and slab break-off are all tectonics features commonly associated with convergent margin interactions, showing that while subduction zones' motions fundamentally shape tectonics settings, their interactions hold the key to their complexities. Fundamental properties such as slab buoyancy, dip direction, and coupled mantle flow determine the motions of single hinge zones. When these zones approach, stress transfers between the slabs through the lithosphere and the mantle, thereby altering the subduction force balance, favoring, opposing, or diverting further motions. We illustrate the range of configurations reported in tectonic reconstructions and address their dynamics through the results of analog and numerical models of subduction dynamics in the upper mantle. The Cenozoic evolution of the Mediterranean provides relevant examples of such interactions, where the coeval activity of several subduction zones during the Africa-Europe convergence has strongly overprinted the current tectonics. A comparison of new analog models with the deep dynamics of the Mediterranean shows how the interactions among slabs and mantle may have shaped the distribution of basins and mountain belts, their uplift, and volcanism in this tectonic province.

1. Introduction

Subduction zones provide the dominant forces for plate tectonics. Wadati-Benioff zones (e.g., Hayes et al., 2018) and the distribution of tomographic anomalies (e.g., van der Meer et al., 2018) provide a snapshot of the present-day conditions characterizing convergent margins and suggest that the cold solid lithosphere sinks into the convective fluid-like mantle with a wide range of dips and shapes. On the contrary, the long-term evolution of subduction is still uncertain and difficult to unravel mainly due to the transient character of the dynamics of the process, influenced by many properties of the system and the possible coexisting, interlinked activity of nearby subduction zones.

Two or more slabs can interact with each other via forces transmitted through both the lithosphere and the mantle (e.g., Jagoutz et al., 2015; Király et al., 2016). Numerical and analog models involving different configurations have shown that the number and the geometry of the interacting slabs strongly affect the overall force balance (Holt et al., 2017; Király et al., 2016, 2018b; Luth et al., 2013; Mishin et al., 2008; Peral et al., 2020; Zhang et al., 2017). As a consequence, interactions of convergent margins can tune trench and subduction velocities, affect slab dips, and enhance local uplifts, plate rotations, and slab break-off.

The coexisting activity of several nearby subduction zones has been proposed to have occurred or still be ongoing in several regions of the Earth (Fig. 1), such as the Mediterranean (e.g. Király et al., 2018a; Vignaroli et al., 2008), Taiwan (e.g., Lallemand et al., 2001), New Zealand (Lamb, 2011), the Molucca Sea (e.g., Amaru, 2007), and around the Philippines plate (Ryukyu vs. Izu-Bonin-Mariana trenches; e.g., Hall, 2002; Ji et al., 2017). However, despite the relevance of this common, yet largely enigmatic process, there is no comprehensive overview of different configurations characterizing past and present-day convergent margins interactions and their dynamic interpretation through modeling.

This work aims to fill this gap, first reviewing the four most commonly applied slab-slab configurations reported in tectonic reconstructions: same-dip, inward-dipping, and outward dipping double subduction, and oppositely dipping adjacent subduction zones (Fig. 2). Then, the dynamics of these configurations are discussed through the combination of published results of analog and numerical models of

* Corresponding author.
E-mail address: agnes.kiraly@geo.uio.no (Á. Király).

https://doi.org/10.1016/j.gloplacha.2021.103501
Received 30 June 2020; Received in revised form 22 February 2021; Accepted 26 April 2021
Available online 30 April 2021

subduction and geological-geophysical data. Finally, ad hoc analog models have been set up to better understand the stress transfer through different media by imposing asymmetry in a double subduction setting. The modeling results contribute to the long-standing debate of coupled 3-D lithospheric, mantle, and surface dynamics characterizing the Cenozoic evolution of the Mediterranean region, where various slab interactions at different depths are reflected by complex long-term surface evolution. The Mediterranean is an ideal test case to study such interactions since the coeval activity of several subduction zones during the convergence between the articulated paleogeographic settings of Africa and Eurasia (Fig. 1) has molded the area, contributing to its current tectonic complexities.

2. Slab-slab interactions

Plate tectonic reconstructions going back up to 500 *Ma* suggest that convergence between plates was often facilitated by multiple subduction zones (Fig. 1*)*. Numerical and analog models illustrate that a relevant process during simultaneously working subduction zones is the stress transfer between the slabs through the lithosphere and the mantle (e.g., Holt et al., 2017; Király et al., 2016; Luth et al., 2013; Peral et al., 2020; Zhang et al., 2017). The type of interaction among slabs can vary depending on the geometry, the properties of the involved lithospheric plates, and the surrounding mantle. In the following sections, we will summarize the four most commonly used, idealized geometries (i.e., same-dip, inward-dipping, outward dipping double subduction and oppositely dipping adjacent subduction zones; Fig. 2) and discuss their dynamics as inferred from geological features and modeling studies.

2.1. Same-dip double subduction (SDDS)

Same-dip double subduction occurs when two parallel subduction zones dip in the same direction (Fig. 2A). Plate reconstruction models show that this configuration is associated with the acceleration of convergence between Eurasia and Africa, Arabia, and India in different periods during the Mesozoic and Cenozoic subduction of the Tethys ocean (e.g., Matthews et al., 2016; Stampfli, 2000) (Fig. 1A). Geological and geophysical observations, including paleolatitudes constrained by paleomagnetic differences between volcanic arcs and ophiolite belts (e.g. Jagoutz et al., 2015), multiple slab remnants identified by seismic tomography models (e.g. Van der Voo et al., 1999), and changes in trench kinematics and deformation regime in the upper plate (Faccenna et al., 2018; Gürer et al., 2016) suggest that the increased convergence rate is usually accommodated by the simultaneous subduction of two or more parallel slabs dipping in the same direction.

At present, we can observe this geometry around the Philippine Sea Plate, where the Ryukyu trench is followed by the Izu-Bonin-Mariana (IBM) trench, both subductions dipping westwards. The IBM subducting margin has been active since ca 52 *Ma* and, for most of its history, it has been retreating (e.g., Faccenna et al., 2009; Hall, 2002). However, the dynamics of the Mariana trench has likely changed between 10 and 5 Ma, as it can be inferred from its motion switching from retreating to

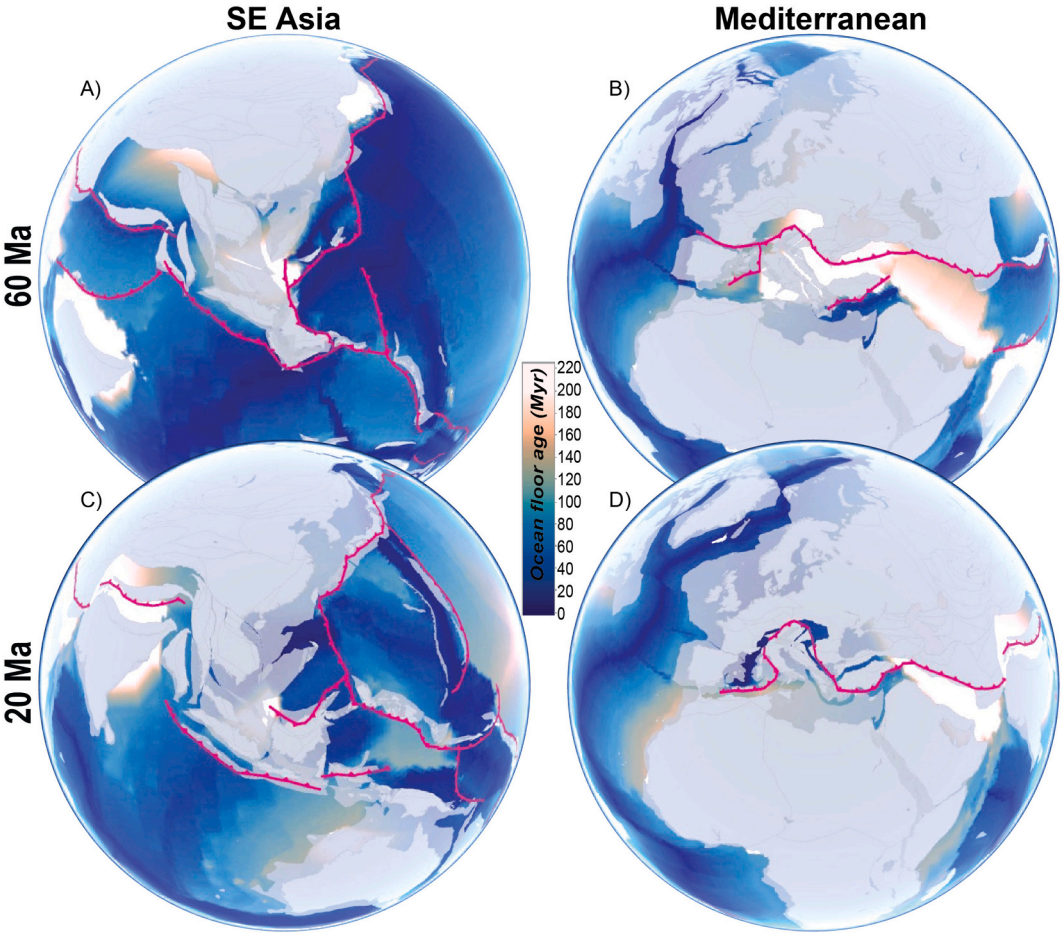

Fig. 1. Global plate reconstruction models suggest many interactions between slabs on a globe, such as in SE-Asia (A&C), and in the Mediterranean (B& D) throughout the recent (<100 Ma) history of the Earth (at 60 Ma – A&B, and 20 Ma – C&D). Grey areas show the continents and the coastlines, and magenta lines represent subduction trenches, and the colored grid shows the ocean floor age at 60 (A, B) and 20 (C, D) Ma (data from Karlsen et al., 2020; Matthews et al., 2016; Müller et al., 2008). (For interpretation of the references to colour in this figure legend, the reader is referred to the web version of this article.)

advancing (Faccenna et al., 2009). This event coincides with the development of the Ryukyu trench and concurrently the double subduction system (Čížková and Bina, 2015; Faccenna et al., 2018). Furthermore, the Ryukyu and IBM subduction zones form a triple junction near Japan where the three subductions interact. This configuration creates a peculiar pattern of seismicity, with deep earthquakes located within the Pacific slab and middle and shallow depth earthquakes within the Philippine slab (Ji et al., 2017).

The idea of two parallel convergent margins, where parts of the Tethys ocean were subducted simultaneously, dates back to the '80s (e.g., Besse and Courtillot, 1988), however geodynamic modeling addressed questions related to this configuration only decades later. Boutelier et al. (2003) studied the convergence and collision of an intra-oceanic arc onto the continent via thermomechanical analog models and found that at the onset of collision a new slab can form in the back-arc region. In their models, same-dip double subduction was a short-lived feature forced by the imposed convergence rate. Mishin et al. (2008) showed in 2D numerical models that the imposed convergence rate largely controls the SDDS, especially the slab geometries and the partitioning of convergence between the two subduction zones. The development of such a SDDS needs tectonic forcing translating into an increased convergence rate which cannot be accommodated by a single subduction zone. Pusok and Stegman (2019) found that a minimum of 5 mm/yr convergence is needed to be imposed for 10 Myrs to initiate the rear subduction and develop self-sustaining SDDS. Once SDDS is initiated it is possible to study the self-dynamic evolution of the system. In the models, the rear subduction is likely to be associated with trench advance, while the front trench can be stationary or retreating, depending on the initial geometry, the rheology, and the properties of the 660 km discontinuity (Čížková and Bina, 2015; Faccenna et al., 2018; Holt et al., 2017; Pusok and Stegman, 2019). This situation is adapted to explain the recent advancing motion of the IBM trench as due to the pull of the frontward Ryukyu trench (Čížková and Bina, 2015; Faccenna et al., 2018; Holt et al., 2018). In particular, Holt et al. (2017, 2018) and Faccenna et al. (2018) related the dipping angle of the slabs to the change in dynamic pressure across both slabs, which is linked to their horizontal migration and the trenches motion on the surface. Independently of the initial slab dip, the region between the two slabs always experiences an increased dynamic pressure, while the front slab has a significant pressure decrease in the mantle wedge area. In contrast, behind the rear slab, there is little dynamic pressure observed (Holt et al., 2017).

2.2. Inward-dipping double subduction (IDDS)

Inward-dipping double subduction occurs when two parallel subduction zones dip in opposite directions towards each other (Fig. 2B). IDDS interactions have been suggested to be relevant in the Caribbean between the Lesser-Antilles and the Central American or part of the Cocos slabs (e.g., van Benthem et al., 2013), in the Philippines between the Manila and the East Luzon subduction zones (e.g., Dasgupta and Mandal, 2018), and in South-East Asia between the Philippine and the Indian plates subduction zones (e.g., Huang et al., 2015; Lyu et al., 2019; Wei et al., 2012). Most of the evidence for IDDS derives from seismic tomography models (Huang et al., 2015) and their combination with plate reconstructions (Hall and Spakman, 2015) and petrological constraints (Wei et al., 2012). Wei et al. (2012) suggest a deep mantle source for magmas in the Hanai Island, which is linked to two distant subductions to the east and west, i.e. to the Manila and the Burma trenches, respectively. However, it needs to be noted that the Manila slab is more likely to dip eastwards, rather than westwards (van der Meer et al., 2018). Inward dipping subduction has been also proposed as the source of mantle upwelling between the proto-Izu-Bonin and proto-W-Philippine trenches, and between the New Hebrides and the Tonga arcs (Faccenna et al., 2010).

The dynamics of IDDS largely depends on the characteristics of the upper plate in between. The length, the elastic thickness, and the rheology of the upper plate regulate the motion of the trenches, and in turn, affect the slabs morphology and the flow patterns of the surrounding mantle (Dasgupta and Mandal, 2018; Lyu et al., 2019). The numerical results of Holt et al. (2017) showed that subduction starting with an initial slab dip of 70• results in slab flattening on the (impermeable) 660 km discontinuity, while in the case of a steeper (95•) initial dip of the slab tips, the slabs develop an overturned geometry, due to the limitation of trench movement at the surface. As flattening on the bottom boundary occurs, slab tips slide towards each other. This condition enhances the development of a small pressure increase in the volume between the two slabs which results in a weak mantle upwelling at the center of the model. Overturned slabs geometry leaves the area between the slabs a neutral zone where negligible mantle flow and dynamic pressure is produced. In models, where the 660 km is not impermeable, slab folding occurring at depth causes alternating periods of overriding plate extension and compression, pairing with small amounts of trench retreat and trench advance, which enhance the slabs folding and time-dependent mantle upwelling (Lyu et al., 2019), confirming what is also observed in single subduction systems (Capitanio et al., 2010).

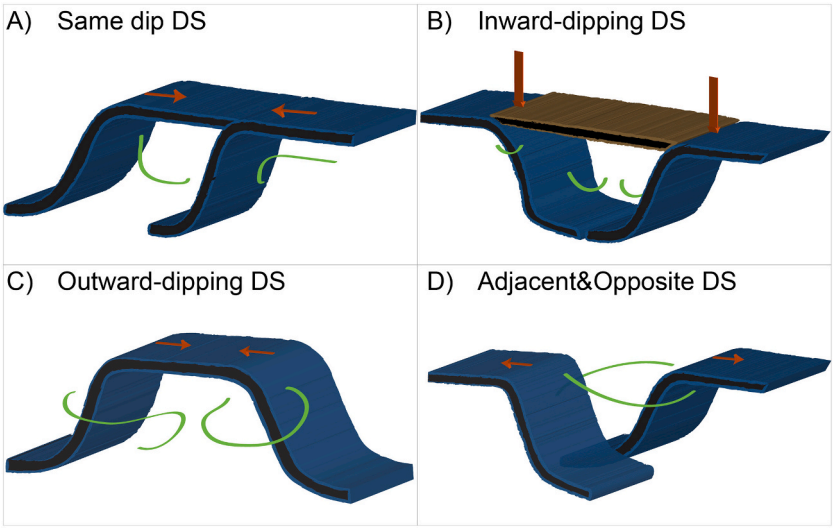

Fig. 2. Illustration of the possible ways of slab-slab interactions and their connections through mantle flow (green lines) and trench kinematics (red arrows). (For interpretation of the references to colour in this figure legend, the reader is referred to the web version of this article.)

2.3. Outward-dipping double subduction (ODDS)

Outward-dipping double subduction occurs when two parallel subduction zones dip in opposite directions away from each other (Fig. 2C). The present-day setting of the Molucca Sea plate is the most well-known example of ODDS. Seismic tomography images clearly show the two opposing-dip slabs (e.g. Amaru, 2007), while on the surface the structures of arc-arc collision are observed (Hall and Smyth, 2008). This geometry has been also suggested in several other places over the geological history of the Earth. For example, the Silurian-Devonian structures of the Lachlan Fold Belt in SE-Australia show many signatures that suggest the activity of at least 2 subduction zones with opposite dips, that the authors called diverging double subduction (Soesoo et al., 1997). The signatures include opposed thrust systems and extensive long-lived granitoid magmatism with mantle signature which evolves to bimodal volcanism. Two opposing magmatic arcs and their soft collision suggest underlying ODDS in Tibet at the Lhasa–Qiangtang collision zone during the Mesozoic (Zhu et al., 2016). In the Mediterranean, the recent tectonic setting involves two active oppositely-dipping subduction zones along the Dinarides - Hellenic arc and the Apennines - Calabrian arc. Going back some millions of years, ODDS extended until the North-Apennines and Dinarides, where the slabs can be still imaged by seismic tomography (Piromallo and Morelli, 2003; Wortel and Spakman, 2000). In the Mediterranean, the ODDS has not reached an arc-arc collision phase, because the northern part of the Adria plate consists of thinned continental lithosphere, with shallow water carbonate platforms (Calcagnile et al., 1982; Royden and Faccenna, 2018), hence, subduction hindered before the two trenches could collide. Towards the south, the Calabrian and the Hellenic arcs are still approaching each other.

The dynamics and effects of ODDS have been extensively studied in the past years employing numerical and analog models. Numerical models showed that in a homogeneous and symmetric setting, as expected, the two trenches have the same velocity and the slabs obtain the same dip angle (Di Leo et al., 2014; Holt et al., 2017). As the slabs approach each other through slab roll-back, the dynamic pressure increases in the mantle between them, which drives the flow of mantle from below the plate outwards (Di Leo et al., 2014; Holt et al., 2017). The seismic anisotropy pattern of this type of flow is substantially different from that created by a single slab, as the dominant fast direction behind the slab is trench parallel instead of trench perpendicular (Di Leo et al., 2014). The increasing dynamic pressure in the sub-slab area resists the slab roll-back, slowing it down when the approaching slabs reach a distance of ~600 km (Király et al., 2018b). When asymmetry is present in the system, the range of interaction modalities broadens. For example, if the initial slab length is different on the two sides, the plate is likely to move towards the longer and faster slab, where the pull is constantly larger, forcing an increased trench retreat rate on the initially slower side (Király et al., 2018b). The motion of the subducting plate is also regulated by the coupling with the overriding plate (Zhang et al., 2017). A larger thickness of the overriding plate increases the coupling between the subducting and the upper plates, offering resistance to the trench mobility. On the contrary, a thinner overriding plate results in lower coupling enhancing deformation and higher trench mobility. Indeed, differences in the overriding plates nature on the two sides of the subducting margins can lead to a significantly asymmetric evolution (Zhang et al., 2017). When an asymmetric setting is instigated by including a sliver of continental lithosphere on one side of the system (i.e. the negative buoyancy of the slab decreases on one side while remains constant on the other), the distance between the slabs at the time of continental subduction proved to be important. If trench distance is less than ~500 km at the onset of continental subduction, the decreased slab-pull and the high dynamic pressure between the two slab hinders the subduction with the continental lithosphere. If the trench distance is larger at the onset of continental subduction only plate movement is expected towards the purely oceanic subduction zone, while the continental sliver is slowly dragged down by the overall negatively buoyant slab (Király et al., 2018b). This suggests that relevant slab interactions occur through both the lithosphere and the mantle.

2.4. Adjacent & oppositely dipping double subduction (AODS)

Adjacent & oppositely dipping double subduction occurs when two nearby subduction zones that dip in opposite directions pass next to each other (Fig. 2). During their migration histories, subduction zones may initiate or come close to each other. Examples of AODS can be found in the European Alps, where oppositely dipping nearby subductions have been proposed in multiple places and times during its evolution. Between the Eastern and the Central Alps tomography models show a reversal in subduction polarity (e.g., Lippitsch et al., 2003; Zhao et al., 2016), which suggests the subduction of the Adriatic lithosphere under the eastern-Alps, while the Eurasian lithosphere is subducted under the Central Alps. Similar polarity reversal was suggested between the Western-Alps and the Apennines subduction zones (e.g., Vignaroli et al., 2008). Between the Alps and the Apennines, the extension of the Voltri Massif, post-orogenic rotations in the Western Alps, and the break-off of the Western-Alps slab have been all connected to the interaction between the slabs through their coupled toroidal flow (Király et al., 2016; Maffione et al., 2008; Molli and Malavieille, 2011; Vignaroli et al., 2008). Molli and Malavieille (2011) pointed out the similarities between the junction of the Alps and the Apennines and the junction of the Ryukyu and Manila subduction zones in Taiwan. In Taiwan, highly curved subduction edges are the result of the interaction of the two subduction zones passing next to each other. Furthermore, the encounter of the subduction edges led to the progressive closure of the South China Sea and an oblique collision between the Eurasian Plate and the Luzon arc resulting in the structures of the Taiwan Island. Subduction style processes are not limited to oceanic subduction, and hence, it is also possible to observe polarity reversal in convergent zones with continental lithospheric subduction, which has been suggested to be the case at the junction between the Hindu Kush and Pamir mountains (Liao et al., 2017).

Both analog and numerical models addressed polarity reversals and the structures and dynamics of AODS. Chemenda et al. (2001) and Luth et al. (2013) both studied the structural elements of convergence accommodated by two oppositely forming slabs by means of analog models. Chemenda et al. (2001) created a setup representing the tectonic setting around Taiwan: two externally forced, adjacent, opposite, and slightly oblique subduction zones on an unrealistically weak mantle (pure water). The setup consists of an oceanic domain with two precut trenches that transitions into a continental margin behind one of the trenches. This setup resulted in roll-back of a purely oceanic slab and significant rotation in the opposite trench, where the slab was partly made of continental lithosphere. In crustal-scale analog models, where AODS starts due to some imposed compression, crustal structures, and uplift-subsidence pattern depend on the initial configuration of, and the distance between, the imposed weak zones (Luth et al., 2013). Subsidence is expected in the transition from one slab edge to the other, while parallel to the slabs a significant number of thrust faults induce uplift (Luth et al., 2013). To better understand the dynamics of slab-slab interactions in fully developed AODS, self-sustaining subduction zones were modeled with lithospheric scale analog and numerical models (Király et al., 2016; Peral et al., 2018). Both works showed the toroidal mantle flow cells connect at different depths throughout the evolution of the models. In Király et al. (2016), we found a critical lateral distance of ~600 km below which the slabs affect each other, exerting reciprocal forcing. The interaction occurs in more curved slab edges on the side of the interaction, a slight change in trench retreat (Peral et al., 2018), and stress-increase close to the slab edges, first at mid mantle depth which then shallows as the slabs move away from each other (Király et al., 2016).

2.5. Common features of slab-slab interactions

The range of forementioned analog and numerical models shows that slabs can interact and affect each other by stress transfer through the mantle and the lithosphere, regardless of the imposed geometry. The characteristic distance of interaction depends on the stress-transferring media. Having weaker rheology, the asthenosphere is marked with a shorter characteristic distance, which is around 500–600 km based on models limited to the upper mantle (Király et al., 2018b, 2016). Slab-slab interaction through the mantle can be observed as an increase of stress (Király et al., 2016) and dynamic pressure (Holt et al., 2017) around the subduction zones, or by a change in the mantle flow pattern (e.g. Di Leo et al., 2014; Peral et al., 2018) concerning those observed in single subduction models. The increase in dynamic pressure on either side of the slabs affects their dip angle and, in turn, the motion of the subduction trenches at the surface (Faccenna et al., 2018; Holt et al., 2018, 2017; Király et al., 2018b). Due to the higher rigidity of the lithosphere with respect to the mantle, the characteristic distance for slab-slab interaction through the lithosphere is likely much higher than the 500–600 km observed for the mantle (e.g. models of Dasgupta and Mandal, 2018 propose an estimation of a couple of thousands of km). Indeed, all subduction zones are coupled as the movement of tectonic plates on the surface of the Earth are not independent of each other. However, the interaction has a clearer signature in some models with movement and deformation of lithospheric plates and change of the trench kinematics (Király et al., 2018b, 2018a; Lyu et al., 2019). These effects are probably best highlighted in asymmetric ODDS models, where the unbalance between slab pull, and the resisting forces between the two sides of subduction clearly induce plate displacements (Király et al., 2018b, 2018a).

3. Analog models of ODDS with imposed asymmetries

Although the studies summarized in the previous sections give an overview of the nature of slab-slab interactions, there are still many gaps in our understanding of such complex systems. For example, the effects of the modified mantle flow pattern on the larger area around double-subduction systems are yet to be understood. From single subduction models, we know that mantle flow around slab edges has a significant vertical component that can be associated with volcanism (e.g., Faccenna et al., 2010; Strak and Schellart, 2014). Similarly to single subduction cases, the mantle flow characterizing a double subduction system might affect volcanism, dynamic topography, and deformations of the overriding- or other nearby plates. Furthermore, models with a single subduction zone showed that the along-trench variability of the subducting plate, or equally the overriding plate, can significantly modify the dynamics of the entire system (e.g. Capitanio et al., 2011; Martinod et al., 2005). Such variations can play an important role in the dynamics of double subduction systems, moreover, the induced deformations, and changes in subduction dynamics might be even more pronounced than in single subduction settings. In the following section, we aim to tighten this gap in our understanding with a new set of ODDS analog models.

3.1. Model setup

Analog models have been used to address a wide range of aspects of slab-slab interactions (e.g., Chemenda et al., 2001; Király et al., 2018b, 2018a; Luth et al., 2013; Peral et al., 2018). Here we present five new models, which, together with the models published in Király et al. (2018b), aim to address the overall dynamics of outward-dipping double subduction systems. We tested asymmetric geometries between the two subduction zones and along the subduction trenches.

Although our models aim to address the fundamentals of slab-slab interactions, the specific geometries were inspired by the complexities of the Adria microplate and its surroundings in the Central Mediterranean (see in the following sections).

To understand the role of such a double subduction system in a larger area, we examine the mantle flow under a laterally placed plate (henceforth lateral plate) in addition to the general description of plate and trench geometries and kinematics. This lateral plate consists of a homogeneous lithosphere in one of the models, while in the other models it has a rigid and a weak part (Fig. 3) to gain more understanding about the interaction between the subduction-induced mantle flow and the lateral plate.

The laboratory models have been performed in an 80 × 80 cm^2 Plexiglas tank, which has been previously filled with a 10 cm thick layer of glucose syrup (Glucosweet 44 - A.D.E.A. srl), representing the upper mantle. Our setup consisted of two lithospheric plates: a subducting plate, on which subduction was induced on two opposite sides, and a lateral plate next to the subducting plate, along the non-subducting northern edge, as illustrated in Fig. 3A. Lithospheric plates were modeled by PDMS silicone mixed with iron fillers which allows regulating both the density and the viscosity of the silicone. To achieve higher viscosity for modeling rigid but light continental lithosphere some silicone was mixed with barite in addition to the iron fillers. The scaling properties of the models can be found in Table 1, and in more detail for each model in the supplementary data (Király et al., 2020a).

The models were monitored by a set of photo cameras, placed around the modeling box: one for a top-view, one for an oblique-view, and one for a lateral view. We switched between two lights at the bottom of the box, allowing us to image two vertical sections: one under the subducting plate and the other under the laterally placed continental plate. The photos were used to track trench geometries and motions, the deformation of the plates, and the mantle flow. For calculating the velocity field in the mantle, we used a particle image velocimetry package (PIVLab) in MATLAB (Thielicke and Stamhuis, 2014). For being able to compare results between the models presented here and the ones in Király et al. (2018b), we normalize the experimental time by the slabs arrival time to the bottom boundary and the trench velocities by the Stokes velocity ($V_{st} = \Delta\rho_{um\text{-}oc} \cdot g \cdot H_{sp} \cdot H_{um}/\eta_{um}$). Abbreviations are listed in the caption of Table 1.

3.2. Model assumptions

The models adopt a set of assumptions based on the overall aims of our study and implied by a number of experimental limitations. Below we list the most important and specific assumptions in the models presented in this work. Further assumptions, such as the impermeable 660 km discontinuity and the lack of temperature gradients, are common in analog models of subduction and they are broadly discussed in many previous studies (e.g. Funiciello et al., 2006, 2003; Király et al., 2018b; Strak and Schellart, 2014).

- No external forces. Subduction is started by pushing down a 3 cm long section on both sides of the subducting plate under the glucose syrup. After the initiation, subduction evolves dynamically without imposing any external forces that could reproduce far-field tectonic forces of the natural prototype.
- No overriding plates. Our model does not include overriding plates. This choice has been made to avoid additional complexities in a setup already intricated. Handling further pieces of lithospheric plate with the risk to enhance the coupling with the lateral- and subducting plate would have increased the possibility of chaotic model evolution. We thus assume that the subduction interface is inherently weak (as weak as the mantle), and thus it is not a primary force in the modeled balance of mature subduction, confirming what was suggested by Zhong and Gurnis (1994) and by Tichelaar and Ruff (1993). This choice may influence the rate of the subduction process but not its general behavior (e.g., Duarte et al., 2013; King and Hager, 1990).

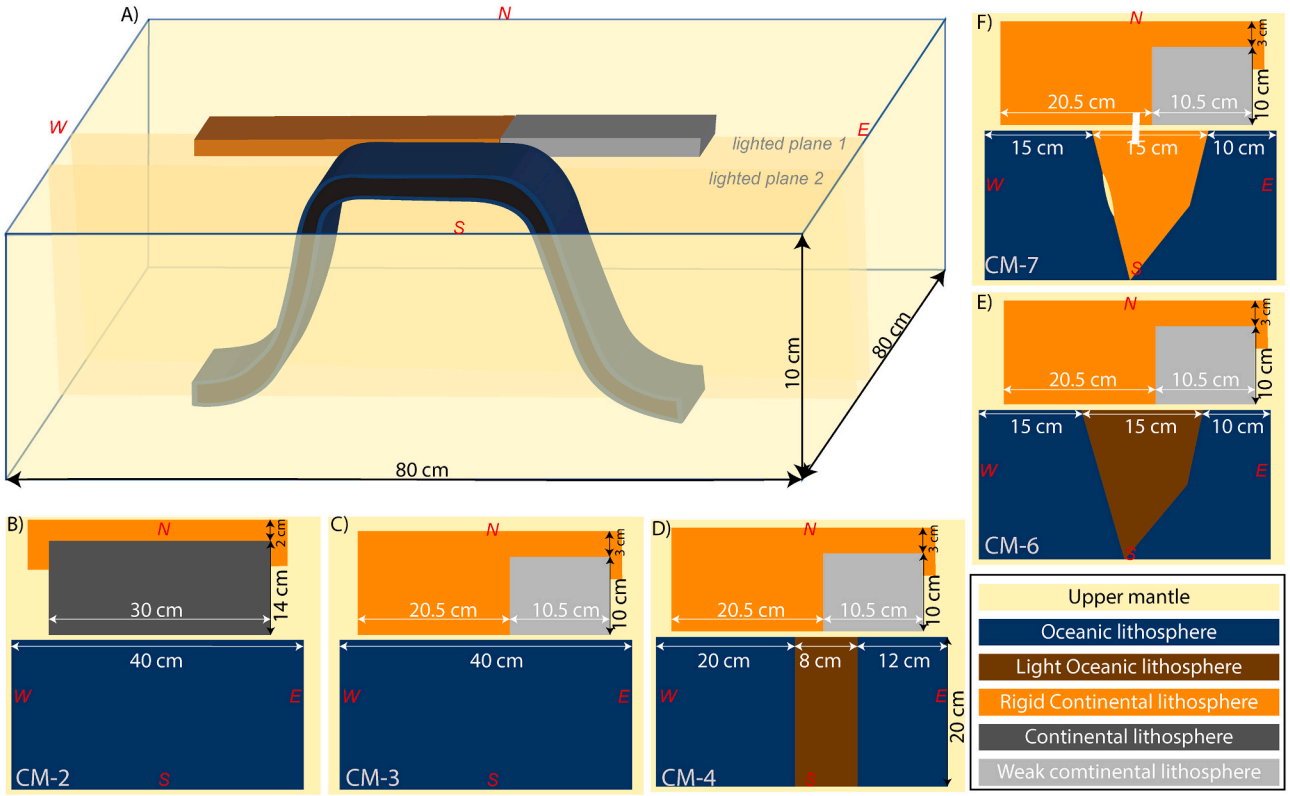

Fig. 3. Analog models setup. A) 3D illustration of the position of the subducting (dark blue) and lateral plates (brown and grey) and the lighted planes where mantle flow is imaged. B—F) Imposed geometry (from top view) of the different silicones in the 5 presented models. The white rectangle on panel F) marks that the lateral and subducting plates were forced to stay close to each other. In each model, subduction is started simultaneously on the W and E edges of the oceanic lithosphere. Refer to Table 1 for the properties of the different silicones used to model the lithospheric plates. (For interpretation of the references to colour in this figure legend, the reader is referred to the web version of this article.)

- The weak zone between the subducting and lateral plates. The characteristics of the used analog materials imply the impossibility to model the weakening mechanisms at the boundary of the subducting plate, which in nature would allow the development of step faults. Experimentally we leave a ~ 0.5 cm layer of glucose syrup between the two plates to prevent possible sticking effects of the two silicon plates.

3.3. Modeling results

3.3.1. Trench geometry and kinematics

The ODDS trench retreat trends are always characterized by 4 typical phases: 1) free sinking of the slabs into the upper mantle; 2) interaction of the slab with the impermeable bottom boundary; 3) "steady-state" roll-back; 4) slow-down of the slabs roll-back due to slab-slab interaction (Király et al., 2018b). In models with homogeneous subducting plates (i.e. CM-2 and CM-3), we observe the same trends for both subduction zones, however, a more pronounced slowdown is observed in phase two, with respect to similar models presented in Király et al. (2018b); e.g. Adria_x3 with 20 cm wide homogeneous subducting plate, without any lateral plate and higher viscosity glucose syrup; Fig. 4A). Furthermore, the normalized velocity amplitudes (i.e. the measured trench velocity/V_{st}) are significantly higher in these new models. Both of these differences derive from the lower viscosity values for the upper mantle in the current models. Because we normalize the velocities with the idealized sinking velocity, the differences in the amplitudes highlight the role of resisting forces (i.e. slab bending and mantle resistance) in a subduction system.

On Fig. 4 *(D—F)*, we show top-view photos of the models CM-3, CM-4, and CM-7 respectively, and the outline of the subducting and lateral plates tracked every 2.5 or 5 min, respectively. Overall, we observe limited deformation in the laterally placed plate. For a homogeneous subducting plate but inhomogeneous lateral plate with weaker material on the eastern side (CM-3), we observe slightly more deformation on the eastern corner, i.e. in the weaker part of the lateral plate. This deformation mainly happens in the final phase of the subduction, when the trenches have well passed the corners of the lateral plate. Furthermore, a slight N-S asymmetry is observed in the evolution of both CM-2 and CM-3, what we consider as the effect of the lateral plate along the northern edge of the subducting plate since this behavior has not been observed in the models without lateral plates in Király et al. (2018b).

The addition of slivers of lighter materials to the subducting plate can either slow or hinder subduction (Király et al., 2018b). In CM4–6 the lighter material has a low, but still negative buoyancy to the mantle, while in CM7 it is positively buoyant (Fig. 3, Table 1).

In CM-4, *E*-W asymmetry is induced by placing the lighter material closer to the eastern edge of the subducting plate. The initiation of the subduction is rather unequal between the two sides, with a faster sinking rate on the western side that resulted in a plate movement towards the west and ultimately a higher peak retreat velocity during the free sinking phase on the eastern side (Fig. 4B). Because of the asymmetric initiation of the process, the two slabs reach the bottom boundary with different angles, which result in higher bending resistance and a larger slowdown for the western slab (that arrives with a higher, almost 90°, angle). After the slabs bending on the bottom, the light oceanic material enters the subduction along the entire length of the eastern trench, causing a significant slowdown of the subduction on this side of the system after ~15 min from the beginning of the model (at ~1.5 normalized time, Fig. 4B). At the same time, the western side remains unchanged with respect to the homogeneous ODDS models (i.e. CM-3).

Table 1
Average scaling properties of the analog models. The experiments are scaled for gravitational and viscous stresses using the buoyancy number Fb = $\Delta\rho_{um\text{-}oc} \cdot g \cdot H_{sp}/\eta_{um}$ (U/L) (e.g., Faccenna et al., 1999), where $\Delta\rho_{um\text{-}oc}$ is the density difference between the lithosphere and the asthenosphere, g the gravitational acceleration, H_{sp} the thickness of the subducting plate, η_{um} the viscosity of the mantle U is a characteristic velocity, and L a characteristic length in the system. A system with a Reynolds number that is << 1 (both in nature and in the models) represents laminar flow. With these parameters, the geometric, kinematic, and dynamic similarity criteria (Hubbert, 1937) are fulfilled.

Symbol	Parameter	Unit	Model	Nature
g	Gravitational acceleration	m s^{-2}	9.81	9.81
	Thickness			
H_{um}	Upper mantle	m	0.1	660,000
H_{sp}	Subducting plate	m	0.0125–0.013	80,000
$H_{lp\text{-}r}$	Lateral plate - rigid	m	0.013	90,000
$H_{lp\text{-}w}$	Lateral plate - weak	m	0.01	66,000
	Length scale		1 cm	66 km
	Width & Length			
$W\&L_{um}$	Upper mantle	m	0.8 & 0.8	5280 000
$W\&L_{sp}$	Subducting plate	m	0.2 & 0.4	1320 000 & 2640 000
$W\&L_{lp\text{-}r}$	Lateral plate - rigid	m	0.12 & 0.20	79,200 & 1320 000
$W\&L_{lp\text{-}w}$	Lateral plate - weak	m	0.12 & 0.10	79,200 & 66,000
	Density			
ρ_{um}	Upper mantle	kg m^3	1422	~3330
ρ_{oc}	Oceanic lithosphere	kg m^3	1481	~3370–3400
$\rho_{light\ oceanic}$	Light oceanic lithosphere	kg m^3	1429	~ 3340
$\rho_{rigid\ cont}$	Rigid continental lithosphere	kg m^3	1392	~3000
$\rho_{continental}$	Continental lithosphere	kg m^3	1372	~2980
$\rho_{weak\ cont.}$	Weak continental lithosphere	kg m^3	1365	~2970
	Viscosity			
η_{um}	Upper mantle	Pa s	73	~10^{20}
$\eta_{oceanic}$	Oceanic lithosphere	Pa s	37,500	~10^{22}–10^{23}
$\eta_{light\ oceanic}$	Light oceanic lithosphere	Pa s	37,000	~10^{22}–10^{23}
$\eta_{rigid\ cont}$	Rigid continental lithosphere	Pa s	47,500	~10^{23}–10^{24}
$\eta_{continental}$	Continental lithosphere	Pa s	37,000	~10^{22}–10^{23}
$\eta_{weak\ cont.}$	Weak continental lithosphere	Pa s	33,500	~10^{21}–10^{22}
Re	Reynolds number $Re = v \cdot l \cdot \Delta\rho \cdot \eta^{-1} << 1$	–	10^{-5}	~10^{-21}
Time scale	$t_{nature}/t_{model} = ((\Delta\rho \cdot g \cdot h)_{model}/(\Delta\rho \cdot g \cdot h)_{nature}) \cdot (\eta_{nature}/\eta_{model})$		1 min	1.85 Myr
Velocity scale	$(V_{model}/V_{nature}) = (t_{nature} \cdot L_{model})/(t_{model} \cdot L_{nature})$		1 mm/min	0.35 cm/yr

The slow-down of the eastern trench has an important effect on the deformation of the laterally placed plate. In CM-4 instead of the small amount of extension of the weaker segment on the east, we observe the rotation of the entire rigid block on the western side after ~20 min from the beginning of the model (Fig. 4E). Similarly to CM-2 and CM-3, during the evolution of CM-4, we observe a slight N-S asymmetry with faster subduction on the southern side that induces plate migration towards the south.

Changing the initial geometry such that the lighter material enters the subduction zone first on the northern segment of the E-dipping trench, and then both the E- and W-dipping trenches reach the light material progressively from the north towards the south (in models CM-6 and CM-7; Fig. 3), produces results with a higher level of complexity. On Fig. 4C&E we show the results of CM-7, where the positively buoyant continental lithosphere produces more pronounced effects in the trench kinematics, and where a slab gap in the center of the western trench has been also included (as a cut in the lithosphere, where Vaseline prevents possible sticking, similarly to the models in Király et al., 2018a; Fig. 3). During the evolution of CM-7, a progressive slow-down is observed initially on the eastern side, first in the north-eastern segment then also in the central segment, followed by the progressive slow-down from north to south on the western side. To the west, in the central part, the subduction of the light material is prevented by a tear, which opens a slab gap as the dense oceanic material subducts and the light continental material remains at the surface. The opening of the slab gap modifies the trench geometry (Fig. 4F) resulting in highly curved double/triple arcs geometry, as shown in Király et al. (2020b, 2018a). In the final phase of the model evolution, the southern segments (which are almost purely oceanic) experience a stronger slow-down with respect to that in the homogeneous case, as they are affected by the increasing amount of subducted buoyant lithosphere in the north-central part of the system, as well as by the slab gap at the western trench. While the plate center experiences little E-W movement, it shows a significant movement towards the south. The southward movement is also dominant in the lateral plate, which is (in this model) forced to stay attached to the subducting plate. However, a minimal amount of block rotation on the western, rigid part of the lateral plate is observed (Fig. 4F).

3.3.2. 3D mantle flow around ODDS

We detail the characteristics of the subduction-induced mantle circulation specifically operating on a vertical plane perpendicular to the trenches of the ODDS placed under the lateral plate (Fig. 3). Initially, this cross-section is about 2 cm away from the edge of the plate, but as the subduction progresses and the trenches develop a curvature, the slab edge moves further away to distances of 3–5 cm from the highlighted cross-section.

First, we describe the complex 3D pattern of the mantle flow in the case of homogeneous (symmetric) ODDS. Using data also from previously published models (Király et al., 2018b), we can build a complex 3D model of the subduction-induced mantle flow, using 4 different cross-sections (Fig. 5). For a homogeneous plate, ODDS induces a strong toroidal mantle flow which is best visible on a horizontal plane that is imaged close to the surface (blue arrows in Fig. 5). In a vertical plane, under the center of the subducting plate, across the two opposite slabs, we can image the mantle poloidal flow pattern (purple arrows on Fig. 5). In the steady-state phase, a mantle return flow starts from the slab tips at depth, moving upwards to the wedge area, and turning to a strong horizontal flow in the top third of the mantle thickness. It corresponds to the strong trench perpendicular mantle flow towards the trenches, which is visible on the top horizontal layer. An important feature of the 3D mantle flow-field is the escape-flow, coming out from below the subducting plate. This flow is driven by the increasing dynamic pressure between the two converging slabs, and hence its intensity increases as the two slabs are approaching each other (Holt et al., 2017; Király et al., 2018b). Here, we add two additional cross-sections to better image the mantle escape-flow. A vertical plane from the edge of the plate, halfway between the two slabs (yellow arrows, Fig. 5) highlights the vertical component of the escape-flow along the central line. The maximum upward flow occurs ~7 cm (= 0.6*mantle depth) away from the plate edge. At distances larger than 7 cm, the mantle outflow is prominently horizontal, moving away from the subducting plate. Perpendicular to this section, we image the mantle escape-flow spreading parallel to the subducting plate (red arrows on Fig. 5). Note that this section has been made under a lateral plate, which has not been present in the models from where the other three cross-sections were derived. This influences the observed velocities close to the surface (i.e. where the PIV images the movements of the plate vs the mantle motion), which are somewhat conflicting with the flow-field observed on the top horizontal layer (blue

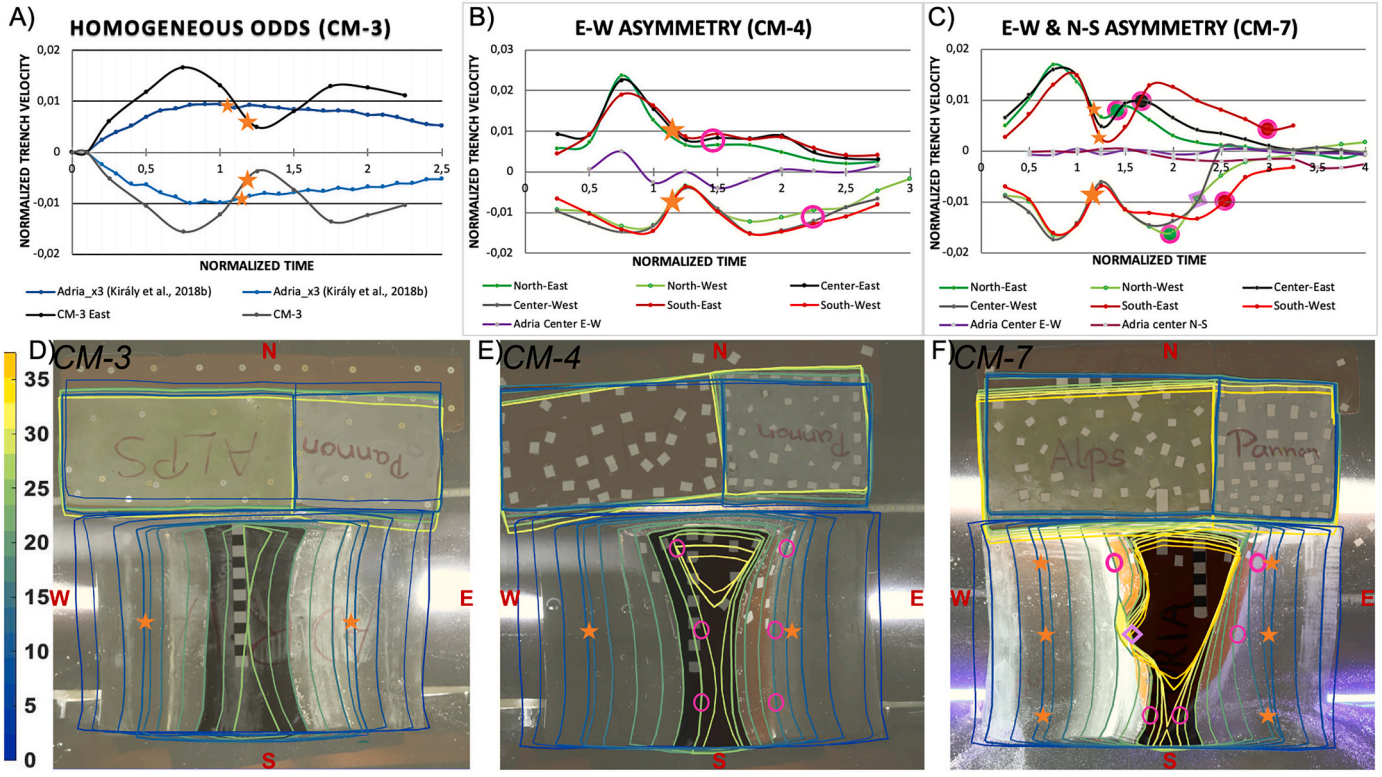

Fig. 4. Trench kinematics and upper plate deformation in the models Adria_x3 (homogeneous ODDS with higher mantle viscosity and without lateral plate from Király et al., 2018b) (A), CM-3 (A, B, D), CM-4 (B, E), and CM-7 (C, F). Imposed geometries for each model are shown in Fig. 3. A-C): Plots showing the trench kinematics (grey-black lines - in the center of the trench, red lines – on the southern segments, green lines – on the northern segments). Positive velocities mean westward movement and northward movement on panel C for "Adria center N-S" (dark magenta). D—F): Top view photos of experiments, with the outline of the subducting plate in every 2.5 min and the outline of the lateral plate in every 5 min (colors are used to show the time progress in minutes, see the colour bar on the left). Both on the top and bottom panels, orange stars mark the time of the slab's interaction with the bottom boundary; pink circles mark the initiation of continental / light oceanic lithosphere subduction and the purple diamond represents the opening of the slab gap in CM-7. (For interpretation of the references to colour in this figure legend, the reader is referred to the web version of this article.)

arrows) without a lateral plate. In general, we observe a diverging mantle flow from the centerline between the two slabs, which turns to an upwelling further away, close to the eastern and western edges of the lateral plate. This mantle flow component eventually combines with the toroidal pattern and turns towards the retreating trench.

Next, we will further discuss the flow on a vertical plane under the laterally placed plate, comparing the results of models with different amounts of asymmetry involved in their setups (Fig. 6). As described above, the mantle flow mapped on this plane is the combination of the escape flow, driven by the gradient of dynamic pressure, and toroidal flow patterns. Examining the time evolution of the horizontal and vertical components of the mantle flow under the lateral plate (averaged over a depth range of ~2 cm starting from below the plate), we observe that the most prominent upwelling always occurs around the edges (E and W) of the lateral plates (Fig. 6, third column). Furthermore, observations show a little effect from the nature of the lateral plate. The differences between CM-2 and CM-3 (differing only in the lateral plate, Fig. 3) are rather derived from the quality of the PIV images (i.e., the slab in the background interferes with the highlighted plane in CM-2), while still showing the same general trends. However, with a careful look, one might notice a small difference of the vertical velocity at the eastern versus the western edges of the lateral plate in CM-3, which is not observed in CM2. In CM-3, the horizontal velocities increase as slabs converge with time, and the two maxima in the horizontal velocity also converge. In contrast, the peaks of the vertical velocity component are always localized at the edge of the lateral plate (marked with magenta dots on Fig. 6), and their amplitude decreases with time. At the same time, the mantle upwelling strengthens in the centerline, and it reaches the same amplitudes at the end of the experiment when the two trenches meet at the surface, and the entire plate sinks.

In CM-4, with imposed *E*-W asymmetry both in the subducting and the lateral plates, the unequal subduction initiation and its consequences (Fig. 4) are well reflected on the horizontal component of the mantle flow under the lateral plate. Initially, the western trench starts faster and the plate moves westward, resulting in slightly higher horizontal velocities towards the west. The interaction with the bottom slows down more the subduction on the west, which is reflected by a much higher amount of mantle flowing towards the east (at 12.5 min). Later there is a slight asymmetry in the flow towards the west, which is the result of the subduction of light oceanic lithosphere along the eastern trench. Interestingly, in this model, the maximum upwelling is also shifted away from the edges, on the east outside of the plate edge, and the west before the lateral plate's edge (Fig. 6).

In the last two experiments, where both E-W and N-S asymmetry has been imposed on the ODDS system we increased the time resolution of the PIV images in the vertical plane under the lateral plate. These results highlight that, after the general slow-down during phase 2, as the light material progressively enters the eastern subduction, the horizontal component of the mantle flow strengthens in this direction, while the vertical component of the flow vanishes on the eastern side while it slightly strengthens - or at least stays constant- on the opposite side (Fig. 6 CM-6 and CM-7). In both models a general slowdown of the velocities is observed from around the time the western trench reaches the lighter material, which induces a decrease in the trench retreat rate in the closer, northern and central segments (at ~25 and ~ 20 min, respectively in CM-6 and CM-7). In CM-7 the positively buoyant segment

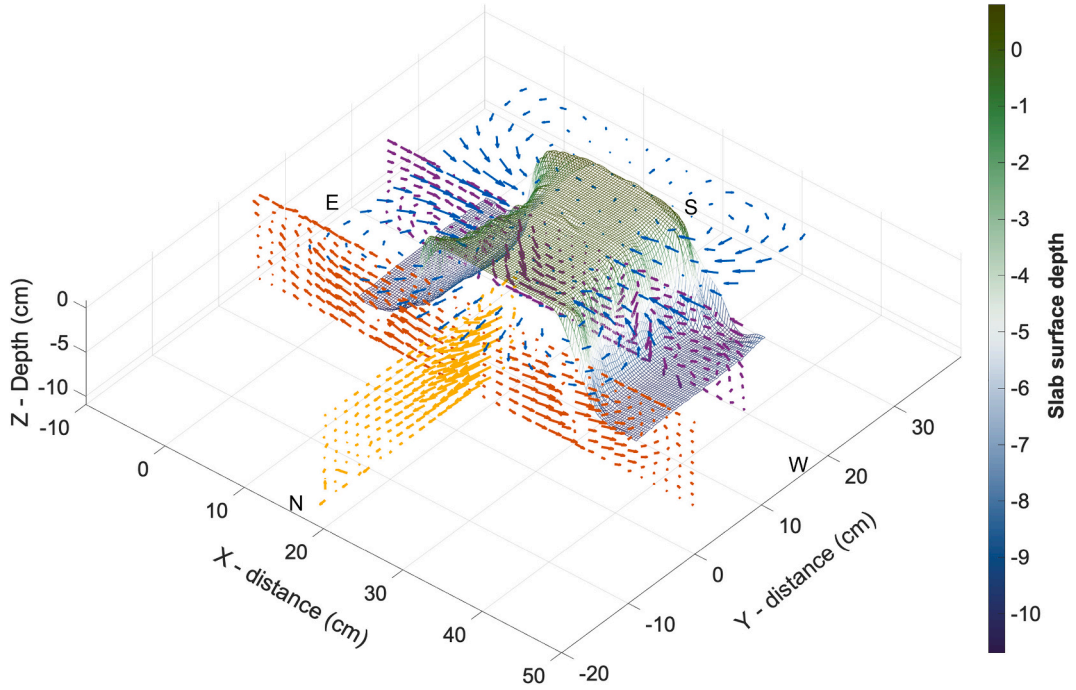

Fig. 5. Mantle flow pattern in 4 different cross-sections using the results from models with 20 cm wide homogeneous ODDS: Adria_3a (blue arrows); Adria_x2 (yellow arrows), Adria_x3 (purple arrows) from Király et al., 2018b; and CM-2 (red arrows)). All cross-sections were taken when the distance between the two trenches was about 12 cm. The mantle flow pattern is calculated by using the PIVlab toolbox in MATLAB (Thielicke and Stamhuis, 2014). The slab surface was detected by 3D laser scanning in the model Adria_x2 (Király et al., 2018b). (For interpretation of the references to colour in this figure legend, the reader is referred to the web version of this article.)

of the subducting plate, as well as the opening slab gap, hinders the subduction in the northern and central segments of both subductions (Fig. 4). The decreasing velocity can also be attributed to the increasing distance between the actively retreating trench segments, the edge of the subducting plate, and the lighted plane. Regardless, we still observe a minimal amount of divergent flow and some upwelling at the western edge of the lateral plate until the end of the experiment, driven by the convergence of the southern segments.

3.4. Summary of the modeling results

The current set of laboratory models furthers our understanding of ODDS systems. The new main outcomes are:

1. The lateral plate has only a small effect on subduction dynamics. In general, we observe that subduction is slightly (~5–15%) slower on the side where a lateral plate is placed (i.e. the northern side) and the subducting plate moves southwards in the late phases of the model evolutions.
2. The deformation of a laterally-placed plate next to a subducting plate depends on both its rheology and the dynamics of the nearby ODDS. Weaker plate segments experience more internal deformation, mostly extension.
3. E-W asymmetry in the subducting plate, which induces decreasing trench retreat on the eastern side, results in the rotation of the western, more rigid part of the lateral plate. This rotation must be attributed to the asymmetric mantle flow (as shown in Király et al., 2018b), induced by the slow-down of the eastern side of the ODDS, since the lateral plate is only connected to the subducting plate through the mantle.
4. The addition of N-S asymmetry in the subducting plate geometry results in southward movement of the subducting plate, and consequently also of the lateral plate. This movement is forced by the increasing slab pull force from north to south.
5. The slow-down of the eastern trench initially increases the horizontal mantle flow towards the east under the later plate. Further decrease in slab roll-back results in the more expected asymmetry in the mantle flow under the lateral plate with the stronger flow on the faster side.
6. The maximum upwelling under the lateral plate occurs at plate edges. This suggests that the upwelling might be the result of edge-driven flow, or more likely the combined effect of the escape-flow turning to toroidal flow and the edge-driven flow.
7. Our results suggest generally a stronger mantle upwelling near the (steeper) edge of the rigid and thick continental plate, independently of the subduction dynamics.

In the following section, these results guide an interpretation of the evolution and present-day settings of the Central Mediterranean (Fig. 7), which provides one of the most remarkable examples of slab-slab interactions.

4. The Central-Mediterranean

In this section, we will shortly summarize the key elements of the Mediterranean tectonic evolution, and point out when slab-slab interactions may have played a significant role. Detailed reviews of the Mesozoic-Cenozoic history of this area can be found in several works (e.g. Faccenna et al., 2014a; Handy et al., 2014; Royden and Faccenna, 2018; van Hinsbergen et al., 2020).

4.1. The evolution of the Central-Mediterranean

The central part of the Mediterranean area represents a tectonically complex region with multiple subduction zones active simultaneously (Figs. 7 and 8). During the Jurassic the closure of an old oceanic basin, the Paleotethys, paired with the opening of a new ocean, the Neotethys (Stampfli, 2000). The closure of the Neotethys has started around 100

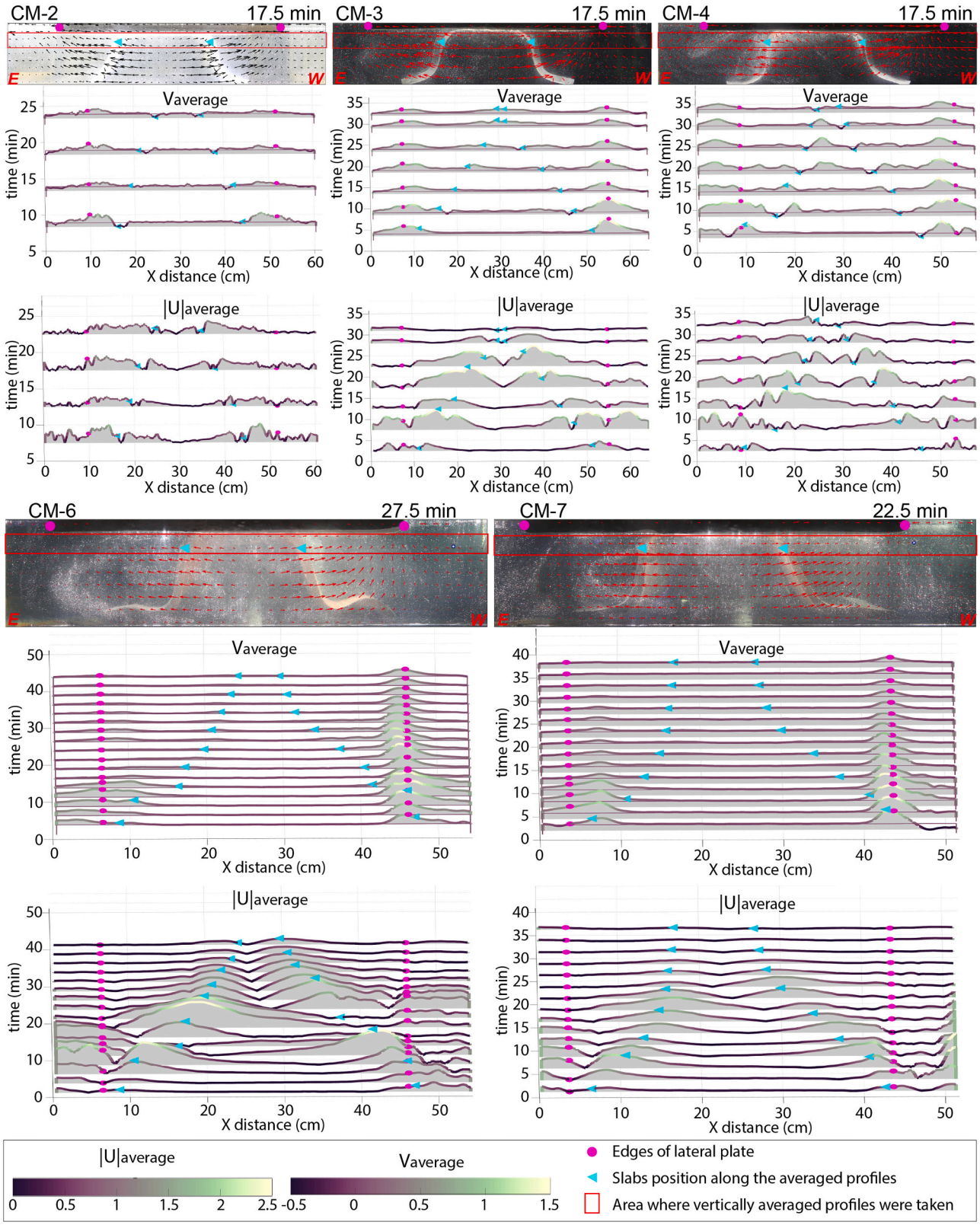

Fig. 6. Cross-sections showing the mantle velocity field under the lateral plate at the "steady-state" phase of subduction. The red boxes show the approximate location where depth-averaged velocities are calculated along the horizontal profile. The horizontal and vertical components of the velocity profiles are plotted separately and for multiple timesteps. Magenta dots mark the edges of the lateral plate, while the cyan triangles mark the approximate position of the slabs behind the highlighted vertical plane. (For interpretation of the references to colour in this figure legend, the reader is referred to the web version of this article.)

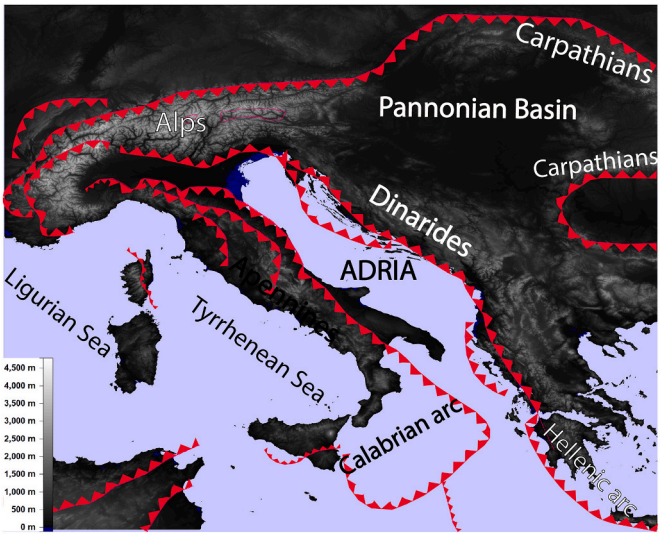

Fig. 7. Topography and present-day tectonics in the central Mediterranean region. The map highlights the sutures of past and present-day subduction zones. DEM data is from the SRTM project (Jarvis et al., 2017). Tectonic elements are based on Faccenna et al. (2014a).

Ma along two opposing subduction fronts: south-dipping subduction under the present day's Alps and east-dipping subduction under the Dinarides (e.g., van Hinsbergen et al., 2020). The initiation of the Alpine subduction has been most likely forced by the increased convergence rate of Africa towards Europe (Gaina et al., 2013), as suggested by the lack of subduction initiation related magmatism (McCarthy et al., 2018). Along most of the Alpine subduction the European plate subducted below Greater Adria, however, towards the west, Greater Adria underthrusted the European margin forming the proto-Apennine slab, and towards the east, the eastern margin of Adria started subducting under Europe forming the Dinarides slab. The Dinarides subduction is dipping towards the east, and hence it was not (or not directly) induced by the N-S convergence between Africa and Europe. During the Cretaceous and Paleocene, there is no significant magmatism along the Alps, while abundant Late-Cretaceous magmatic activity characterizes the Dinaric margin, suggesting that the slab rolled back shortly after subduction initiated (Toljić et al., 2018; Ustaszewski et al., 2009).

A characteristic change in the Central Mediterranean tectonics occurred around the Late Eocene- Oligocene (i.e. 35–30 *Ma*; Fig. 8A). Along the Alpine and Dinaric margin, the accretion of Greater Adria caused a soft collision between Adria and Europe. At the same time, the shallow dipping proto-Apennine slab evolved into a fully-fledged subduction, producing arc magmatism from ~38 *Ma* (e.g., Beccaluva et al., 1989; Faccenna et al., 2001). The Apennines slab roll-back opened two back-arc basins, first the Liguro-Provencal basin (Fig. 8B-C) and subsequently the Tyrrhenian basins (Fig. 8D) (e.g., Faccenna et al., 2001; Malinverno and Ryan, 1986). While most of the Alpine subduction hindered, and some of the Alpine slab broke-off during the Late Eocene - Oligocene, the eastern edge of the Alpine subduction propagated into the Carpathian Embayment (Royden and Faccenna, 2018). The Carpathian subduction also created slab roll-back and opened the Pannonian back-arc basin. Similarly to the Alps, slab-break-off happened along (at least) some parts of the Dinarides, pairing with the emplacement of Oligocene granitoids in the inner Dinarides (Schefer et al., 2011). South from the Dinarides, oceanic subduction with slab roll-back continued along the Hellenic arc.

By the end of the Miocene, the Carpathian slab had finished its roll-back, and the slab started to break-off. Progressively younging volcanism towards the south in the Eastern-Carpathians suggests the southwards propagation of a slab tear. At present, seismicity and seismic tomography show a slab that might be in the process of breaking off at

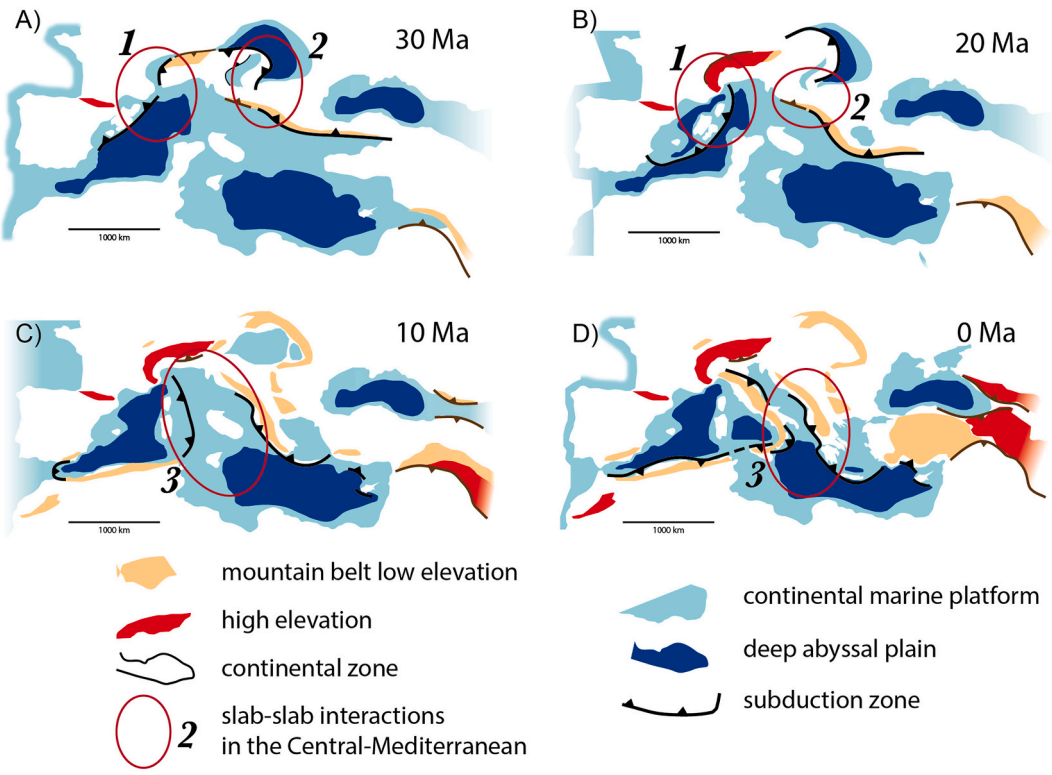

Fig. 8. Tectonic evolution of the Mediterranean, modified after Royden and Faccenna (2018). Red circles show key areas where slab-slab interaction has been relevant in the Central Mediterranean (1: AODS at the Alps-Apennines junction; 2: AODS at the Carpathians-Dinarides junction; 3: ODDS between the Apennine-Calabria and Dinarides-Hellenic arcs). (For interpretation of the references to colour in this figure legend, the reader is referred to the web version of this article.)

the Vrancea zone in the SE-Carpathians. Most of the Apennines slab had also encountered continental lithospheres (Sun et al., 2019), and in the last few millions of years, oceanic subduction occurred only along the Calabrian arc (Fig. 8D). South from the Calabrian arc, a slab tear has formed along the African margin from the Tortonian onward (Faccenna et al., 2005). North from Calabria, slab detachment has occurred in the Central Apennines about 2 *Ma* (Faccenna et al., 2014b; San Jose et al., 2020), while in the Northern-Apennines, the subduction trench encountered with the continental lithosphere that might have caused the subducting plate delamination (Magni and Király, 2019), allowing for the Adriatic mantle lithosphere to peel-off in a subduction roll-back style process (Chiarabba et al., 2014).

Present-day seismic tomography images suggest that in the southern-Dinarides the slab is continuous until 450 km depth, however a break in the slab dip is interpreted around 200 km depth (Šumanovac et al., 2017). In contrast, Bennett et al. (2008) presents a different cross-section, based on the model of Piromallo and Morelli (2003), where the slab only reaches a depth of 200 km. It suggests that even in places where the older slab detached, convergence continued during Neogene, forcing ca. 160–200 km continental subduction (Bennett et al., 2008) or delamination of the Adriatic lithospheric mantle (Schefer et al., 2011).

The current geodynamic setting in the Central Mediterranean can be imaged by seismic tomography models. Several regional models aimed to differentiate slabs and slab segments in this complex area (Blom et al., 2019; Piromallo and Morelli, 2003; Wortel and Spakman, 2000), interpret present-day mantle flow patterns from seismic anisotropy measurements (Margheriti et al., 2014; Salimbeni et al., 2018; Subašić et al., 2017) and draw an interpretation of the slabs position and the related mantle flow (Faccenna et al., 2014a; Király et al., 2018a). These interpretations suggest a mantle flow pattern, which is connecting the different regions of the Mediterranean. The interaction between different slab segments is well reflected by the complex seismic anomalies, variable topography, and tectonic features.

4.2. Role of slab-slab interactions in the Central Mediterranean

Unlike most parts of the Tethys suture zones, the Mediterranean is not characteristic for same-dip double subduction, instead, the much shorter subduction zones create the possibility of interactions in outward-dipping and adjacent & oppositely dipping geometries (Fig. 8).

AODS geometry can be identified multiple times during the evolution of the region (e.g. van Hinsbergen et al., 2020). For example, at the Cretaceous initiations of the Neotethys subduction segments, the Alpine and Dinarides slabs developed adjacent to each other, with opposing dip directions. However, to date, there is no study showing geological evidence suggesting that they had any effect on each other or the area around the junction of the two trenches. In contrast, multiple evidence suggests strong interactions between the Western-Alps and the Apennines during the Late Paleogene – Neogene (number 1 on Fig. 8). The abundant geological evidence combined with geodynamic modeling revealed two main effects of the interaction between the two slabs. The timing of the first deepening of the Apennine slab in the Early Eocene, coincides with the proposed break-off of the Alpine slab started under the Western-Alps (von Blackenburg and Davies, 1995), and the related uplift that shows in the peak of metamorphism and in the change of transport directions of the Alpine tectonic units (Handy et al., 2010). Numerical models suggest that when the two adjacent slabs are in line with each other, there is a significant stress increase around the slabs at 250–500 km depth (Király et al., 2016), which could potentially aid slab-break-off. Geodynamic models also showed that in a later phase when slabs diverge from each other due to slab roll-back, the toroidal flow around the slab edges connect and create a high shear stress area close to the surface, in between the two subduction zones (Király et al., 2016; Peral et al., 2018). The high stress in the top of the asthenosphere can induce rotations, and increase the curvature of the nearby slab edges of the two subduction zones. Indeed, the W-Alps obtained its highly curved geometry very late in its evolution, between 30 and 10 *Ma* (Collombet et al., 2002; Maffione et al., 2008), when the Apennines trench retreated quickly, diverging from the structured Alpine subduction (Vignaroli et al., 2008). In between the W-Alps and N-Apennines, a peak of rotation is shown by paleomagnetic measurements around 30 *Ma*, but further rotations have occurred also during the Miocene (Maffione et al., 2008). Furthermore, Vignaroli et al. (2008) suggested that in the Alps-Apennines junction, the Ligurian Alps has undergone significant extension driven by the roll-back of the Apennines slab. At present, strong seismic anisotropy is observed in the asthenosphere between the W-Alps and N-Apennines, suggesting a flow which is in agreement with what is found in numerical models (Király et al., 2016; Salimbeni et al., 2018).

AODS geometry is proposed by tectonic reconstructions (Royden and Faccenna, 2018; van Hinsbergen et al., 2020) also at the junction of the Carpathian and the Dinarides subduction zones from the Late Eocene onward (number 2 on Fig. 8*)*. However, no previous work addressed the tectonic implications of the configuration of these two subduction zones.

The present-day geometry of slabs gives clear evidence for ODDS on the two sides of Adria (Faccenna et al., 2014a; Király et al., 2018a; number 3 on Fig. 8). This ODDS system is tectonically very complex, as the subducting lithosphere is not entirely oceanic, with continental subduction either converting to the delamination of the mantle lithosphere (and maybe parts of the lower crust) or causing slab detachment and the opening of a gap (Chiarabba et al., 2014; Faccenna et al., 2014b; Sun et al., 2019). Due to the ambiguous data on the style of the Neogene subduction along the Dinarides, and on the composition of the Adria microplate, it is difficult to predict whether the subduction zones affected the trench kinematics on the opposite sides. Our modeling results propose that the asymmetric evolution between the Apennines and Dinarides slab resulted in a strengthened mantle flow towards the west, which might have further helped the Eocene rotation of the Western Alps, that has been likely driven by the Apennines slab roll-back in relation to the AODS system. This strong toroidal flow under the Alps and towards the Apennines is preserved by the alignment of mantle olivine, creating remarkable seismic anisotropy pattern (Salimbeni et al., 2018).

The SKS fast directions along the Calabrian arc and N-Apennines are parallel to the trench and the slab. The slab parallel anisotropy has been originally interpreted as an anisotropic texture within the slab (Margheriti et al., 2003), however, it is also consistent with the mantle flow which is characteristic for ODDS (Di Leo et al., 2014). The trench parallel anisotropic direction is likely produced by the escape-flow, which is driven by the increasingly high pressure between the slabs. As we showed in this study, the escape-flow is predominantly a divergent flow with strong horizontal and some vertical components (Fig. 5).

In the present models, we observed most of the mantle upwelling around the edge of the lateral plate, suggesting that the upward flow away from the centerline in between the slabs is at least partly edge-driven. This finding corresponds with the suggestions of Harangi et al. (2015), who proposed that the Late-Miocene-Pliocene (11–0.1 *Ma*), low volume basalt-volcanoes, which are scattered around the W-NW edge of the Pannonian basin, were produced by asthenospheric upwelling along the shallowing lithosphere from the thickened Alpine to the thinned Pannonian lithosphere (Harangi et al., 2015). Such a lithospheric step (>60 km; Horváth et al., 2006) can force an asthenospheric flow to upward motions, which can induce decompression melting and volcanism (Davies and Rawlinson, 2014; Harangi et al., 2015). The basaltic volcanism cannot be the result of slab-roll-back and back-arc basin opening, that occurred during the Early Miocene (Horváth et al., 2006, 2015). On the other hand, roll-back subduction was still active along with the Apennines slab during the basaltic volcanism, which could have created enough pressure under the Adria plate to drive mantle flow towards the Pannonian basin. At present, as convergence is still active in the southern segments of the ODDS, a weak escape-flow is still expected from below Adria towards the Alps and the Pannonian Basin. The

upwelling related to this escape-flow might contribute to the recent uplift of the Alps, which has been suggested to be partly driven by asthenospheric flow (Sternai et al., 2019), and it might support the positive dynamic topography of the Pannonian Basin (Faccenna et al., 2014a). Note, that the escape flow might be stronger than in the latest evolution of model CM-7 (Fig. 6), as we expect that subduction style delamination in the N-Apennines (Chiarabba et al., 2014) enhances the asthenospheric flow.

An important addition to the outward-dipping double subduction system of the Adria plate is the opening of a slab gap under the Central-Apennines. The cessation of subduction and the consequent slab break-off occurred ~2 *Ma*, resulting in rapid (>0.5 km/My) surface uplift (San Jose et al., 2020), and the curvature of the Apennine-Calabria arcs (Cifelli et al., 2007; Lucente and Speranza, 2001; Speranza et al., 1997). Furthermore, the location of the gap in the slab, that is imaged by many seismic tomography models (Piromallo and Morelli, 2003; Wortel and Spakman, 2000), coincides with the area where the seismic anisotropy pattern is showing multiple directions with a high angle to the previous trench, unlike other parts, where the fast directions are primarily parallel to the slab (see compilation in Faccenna et al., 2014a). The location of the slab gap further coincides with the area where recent internal deformation is observed in the Adria Plate (D'Agostino et al., 2008; Király et al., 2018a). Previous modeling works showed that, when the slab detaches close to the surface, the ensuing opening gap modifies both the mantle flow and the surface trench geometry (Király et al., 2018a, 2020b), corresponding well to the topography of the Apennines and the disturbed SKS pattern around the area, where the slab is missing. In a double subduction system, the multiple curvatures of the affected trench seem more long-lasting, and the mantle flow through the slab window is stronger, due to the increased pressure difference across the slab. The models also suggest the internal deformation of the subducting plate and plate movement towards the opposite trench during the slab gap opening, which is consistent with recent GPS measurements (e.g. Serpelloni et al., 2013).

5. Final remarks

The subduction of lithospheric plates induces stress and related deformation in the surrounding mantle and the nearby lithospheric plates. It follows that, when subduction zones operate close to others, their dynamics change, reflecting the stress transfer from nearby slabs (Király et al., 2016). The effect of slab-slab interactions can show in the trench movement, in the mantle flow pattern, and in the deformation and uplift history of the area around and between subduction zones. We showed that slab-slab interactions have likely occurred throughout the history of recent tectonics in many convergent zones. The recent evolution of the Mediterranean area is a great example of complex tectonic history, comprising the simultaneous subduction of multiple slabs during the slow convergence between Africa-Adria and Europe. Our present modeling effort clearly showed that the outward-dipping double subduction of Adria produces wide-spread mantle flow which can contribute to the deformation, uplift, and magmatic activity of the nearby tectonic plates.

Research data and supplementary materials

Data created during the processing of the analog models is available in the EPOS database platform (Király et al., 2020a).

Declaration of competing interest

The authors declare that they have no known competing financial interests or personal relationships that could have appeared to influence the work reported in this paper.

Acknowledgments

The collaboration on resolving the dynamic interactions between the Mediterranean subduction zones has been initiated by Frank Horváth. Frank was a great mentor, an outstanding solid-earth scientist, able to combine geophysical data with geological reconstruction to build up ground-breaking geodynamic models. Frank created a school of excellence at Budapest working and providing a new vision on the Pannonian and Mediterranean geodynamics, a great scientist and unique friend.

The authors are grateful to J. Duarte and two anonymous reviewers for their thorough review. Their comments and suggestions largely improved the flow of this paper.

This work was supported by the EPOS (TNA laboratory access scheme) and by the Research Council of Norway (Centres of Excellence project 223272). The grant to Dipartimento di Scienze, Università degli Studi Roma Tre MIUR-Italy (Dipartimenti di Eccellenza, articolo 1, commi 314–337 legge 232/2016) is also gratefully acknowledged.

References

Amaru, M.L., 2007. Global Travel Time Tomography with 3-D Reference Models [WWW Document]. Geologica Ultraiectina, URL. http://dspace.library.uu.nl/handle/1874/19338 (accessed 8.4.19).

Beccaluva, L., Brotzu, P., Macciotta, G., Morbidelli, L., Serri, G., 1989. Cainozoic tectono-magmatic evolution and inferred mantle sources in the Sardo-Tyrrhenian area. The Lithosphere in Italy. Adv. Earth Sci. Res. 229–248.

Bennett, R.A., Hreinsdóttir, S., Buble, G., Bašić, T., Bačić, Ž., Marjanović, M., Casale, G., Gendaszek, A., Cowan, D., 2008. Eocene to present subduction of southern Adria mantle lithosphere beneath the Dinarides. Geology 36, 3–6. https://doi.org/10.1130/G24136A.1.

Besse, J., Courtillot, V., 1988. Paleogeographic maps of the continents bordering the Indian Ocean since the Early Jurassic. J. Geophys. Res. Solid Earth 93, 11791–11808. https://doi.org/10.1029/JB093iB10p11791.

Blom, N., Gokhberg, A., Fichtner, A., 2019. Seismic waveform tomography of the Central and Eastern Mediterranean upper mantle (preprint). In: Tectonic Plate Interactions, Magma Genesis, and Lithosphere Deformation at all Scales/Seismics, Seismology, Geoelectrics, and Electromagnetics/Seismology. https://doi.org/10.5194/se-2019-152.

Boutelier, D., Chemenda, A., Burg, J.-P., 2003. Subduction versus accretion of intra-oceanic volcanic arcs: insight from thermo-mechanical analogue experiments. Earth Planet. Sci. Lett. 212, 31–45. https://doi.org/10.1016/S0012-821X(03)00239-5.

Calcagnile, G., D'Ingeo, F., Farrugia, P., Panza, G.F., 1982. The lithosphere in the Central-Eastern Mediterranean area. PAGEOPH 120, 389–406. https://doi.org/10.1007/BF00877044.

Capitanio, F.A., Stegman, D.R., Moresi, L.N., Sharples, W., 2010. Upper plate controls on deep subduction, trench migrations and deformations at convergent margins. Tectonophysics 483, 80–92. https://doi.org/10.1016/j.tecto.2009.08.020.

Capitanio, F.A., Faccenna, C., Zlotnik, S., Stegman, D.R., 2011. Subduction dynamics and the origin of Andean orogeny and the Bolivian orocline. Nature 480.

Chemenda, A.I., Yang, R.K., Stephan, J.F., Konstantinovskaya, E.A., Ivanov, G.M., 2001. New results from physical modelling or arc-continent collision in Taiwan: Evolutionary model. Tectonophysics 333, 159–178. https://doi.org/10.1016/S0040-1951(00)00273-0.

Chiarabba, C., Giacomuzzi, G., Bianchi, I., Agostinetti, N.P., Park, J., 2014. From underplating to delamination-retreat in the northern Apennines. Earth Planet. Sci. Lett. 403, 108–116. https://doi.org/10.1016/j.epsl.2014.06.041.

Cifelli, F., Mattei, M., Rossetti, F., 2007. Tectonic evolution of arcuate mountain belts on top of a retreating subduction slab: the example of the Calabrian Arc. J. Geophys. Res. Solid Earth 112, 1–20. https://doi.org/10.1029/2006JB004848.

Čížková, H., Bina, C.R., 2015. Geodynamics of trench advance: Insights from a Philippine-Sea-style geometry. Earth Planet. Sci. Lett. 430, 408–415. https://doi.org/10.1016/j.epsl.2015.07.004.

Collombet, M., Thomas, J.C., Chauvin, A., Tricart, P., Bouillin, J.P., Gratier, J.P., 2002. Counterclockwise rotation of the western Alps since the Oligocene: new insights from paleomagnetic data. Tectonics 21. https://doi.org/10.1029/2001TC901016.

D'Agostino, N., Avallone, A., Cheloni, D., D'Anastasio, E., Mantenuto, S., Selvaggi, G., 2008. Active tectonics of the Adriatic region from GPS and earthquake slip vectors. J. Geophys. Res. Solid Earth 113, 1–19. https://doi.org/10.1029/2008JB005860.

Dasgupta, R., Mandal, N., 2018. Surface topography of the overriding plates in bi-vergent subduction systems: A mechanical model. In: Tectonophysics, Understanding Geological Processes Through Modelling - A Memorial Volume honouring Evgenii Burov, 746, pp. 280–295. https://doi.org/10.1016/j.tecto.2017.08.008.

Davies, D.R., Rawlinson, N., 2014. On the origin of recent intraplate volcanism in Australia. Geology 42, 1031–1034. https://doi.org/10.1130/G36093.1.

Di Leo, J.F., Walker, A.M., Li, Z.H., Wookey, J., Ribe, N.M., Kendall, J.M., Tommasi, A., 2014. Development of texture and seismic anisotropy during the onset of subduction. Geochem. Geophys. Geosyst. 15, 192–212. https://doi.org/10.1002/2013GC005032.

Duarte, J.C., Schellart, W.P., Cruden, A.R., 2013. Three-dimensional dynamic laboratory models of subduction with an overriding plate and variable interplate rheology. Geophys. J. Int. 195, 47–66. https://doi.org/10.1093/gji/ggt257.

Faccenna, C., Giardini, D., Davy, P., Argentieri, A., 1999. Initiation of subduction at Atlantic-type margins: insights from laboratory experiments. J. Geophys. Res. Solid Earth 104 (B2), 2749-2766.

Faccenna, C., Becker, T.W., Lucente, F.P., Jolivet, L., Rossetti, F., 2001. History of subduction and back-arc extension in the Central Mediterranean. Geophys. J. Int. 145, 809–820. https://doi.org/10.1046/j.0956-540X.2001.01435.x.

Faccenna, C., Civetta, L., D'Antonio, M., Funiciello, F., Margheriti, L., Piromallo, C., 2005. Constraints on mantle circulation around the deforming Calabrian slab. Geophys. Res. Lett. 32, 1–4. https://doi.org/10.1029/2004GL021874.

Faccenna, C., Di Giuseppe, E., Funiciello, F., Lallemand, S., van Hunen, J., 2009. Control of seafloor aging on the migration of the Izu–Bonin–Mariana trench. Earth Planet. Sci. Lett. 288, 386–398. https://doi.org/10.1016/j.epsl.2009.09.042.

Faccenna, C., Becker, T.W., Lallemand, S., Lagabrielle, Y., Funiciello, F., Piromallo, C., 2010. Subduction-triggered magmatic pulses: a new class of plumes? Earth Planet. Sci. Lett. 299, 54–68. https://doi.org/10.1016/j.epsl.2010.08.012.

Faccenna, C., Becker, T.W., Auer, L., Billi, A., Boschi, L., Brun, J.P., Capitanio, F.A., Funiciello, F., Horvàth, F., Jolivet, L., Piromallo, C., Royden, L., Rossetti, F., Serpelloni, E., 2014a. Mantle dynamics in the Mediterranean. Rev. Geophys. 52, 283–332. https://doi.org/10.1002/2013RG000444.Received.

Faccenna, C., Becker, T.W., Miller, M.S., Serpelloni, E., Willett, S.D., 2014b. Isostasy, dynamic topography, and the elevation of the Apennines of Italy. Earth Planet. Sci. Lett. 407, 163–174. https://doi.org/10.1016/j.epsl.2014.09.027.

Faccenna, C., Holt, A.F., Becker, T.W., Lallemand, S., Royden, L.H., 2018. Dynamics of the Ryukyu/Izu-Bonin-Marianas double subduction system. In: Tectonophysics, Understanding Geological Processes through Modelling - A Memorial Volume honouring Evgenii Burov, 746, pp. 229–238. https://doi.org/10.1016/j.tecto.2017.08.011.

Funiciello, F., Faccenna, C., Giardini, D., Regenauer-Lieb, K., 2003. Dynamics of retreating slabs: 2. Insights from three-dimensional laboratory experiments. J. Geophys. Res. 108, 1–16. https://doi.org/10.1029/2001JB000896.

Funiciello, F., Moroni, M., Piromallo, C., Faccenna, C., Cenedese, A., Bui, H.A., 2006. Mapping mantle flow during retreating subduction: laboratory models analyzed by feature tracking. J. Geophys. Res. Solid Earth 111, 1–16. https://doi.org/10.1029/2005JB003792.

Gaina, C., Torsvik, T.H., van Hinsbergen, D.J.J., Medvedev, S., Werner, S.C., Labails, C., 2013. The African Plate: A history of oceanic crust accretion and subduction since the Jurassic. In: Tectonophysics, Progress in understanding the South Atlantic Margins, 604, pp. 4–25. https://doi.org/10.1016/j.tecto.2013.05.037.

Gürer, D., van Hinsbergen, D.J.J., Matenco, L., Corfu, F., Cascella, A., 2016. Kinematics of a former oceanic plate of the Neotethys revealed by deformation in the Ulukışla basin (Turkey) [WWW Document]. Tectonics. https://doi.org/10.1002/2016TC004206.

Hall, R., 2002. Cenozoic geological and plate tectonic evolution of SE Asia and the SW Pacific: Computer-based reconstructions, model and animations. J. Asian Earth Sci. 20, 353–431. https://doi.org/10.1016/S1367-9120(01)00069-4.

Hall, R., Smyth, H.R., 2008. Cenozoic arc processes in Indonesi : Identifi cation of the key infl uences on the stratigraphic record in active volcanic arcs. In: Formation and Applications of the Sedimentary Record in Arc Collision Zones: Geological Society of America Special Paper, 436, pp. 27–54. https://doi.org/10.1130/2008.2436(03), 2436.

Hall, R., Spakman, W., 2015. Mantle structure and tectonic history of SE Asia. Tectonophysics 658, 14–45. https://doi.org/10.1016/j.tecto.2015.07.003.

Handy, M.R., Schmid, M., Bousquet, R., Kissling, E., Bernoulli, D., 2010. Reconciling plate-tectonic reconstructions of Alpine Tethys with the geological-geophysical record of spreading and subduction in the Alps. Earth Sci. Rev. 102, 121–158. https://doi.org/10.1016/j.earscirev.2010.06.002.

Handy, M.R., Ustaszewski, K., Kissling, E., 2014. Reconstructing the Alps–Carpathians–Dinarides as a key to understanding switches in subduction polarity, slab gaps and surface motion. Int. J. Earth Sci. 104 https://doi.org/10.1007/s00531-014-1060-3.

Harangi, S., Jankovics, M.É., Sági, T., Kiss, B., Lukács, R., Soós, I., 2015. Origin and geodynamic relationships of the late Miocene to Quaternary alkaline basalt volcanism in the Pannonian basin, eastern–Central Europe. Int. J. Earth Sci. (Geol. Rundsch) 104, 2007–2032. https://doi.org/10.1007/s00531-014-1105-7.

Hayes, G.P., Moore, G.L., Portner, D.E., Hearne, M., Flamme, H., Furtney, M., Smoczyk, G.M., 2018. Slab2, a comprehensive subduction zone geometry model. Science 362, 58–61. https://doi.org/10.1126/science.aat4723.

Holt, A.F., Royden, L.H., Becker, T.W., 2017. The Dynamics of double Slab Subduction. Geophys. J. Int. 209, 250–265. https://doi.org/10.1093/gji/ggw496.

Holt, A.F., Royden, L.H., Becker, T.W., Faccenna, C., 2018. Slab interactions in 3-D subduction settings: the Philippine Sea Plate region. Earth Planet. Sci. Lett. 489, 72–83. https://doi.org/10.1016/j.epsl.2018.02.024.

Horváth, F., Bada, G., Szafián, P., Tari, G., Ádám, A., Cloetingh, S., 2006. Formation and deformation of the Pannonian Basin: constraints from observational data. Geol. Soc. Lond. Mem. 32, 191–206. https://doi.org/10.1144/GSL.MEM.2006.032.01.11.

Horváth, F., Musitz, B., Balazs, A., Vigh, A., Uhrin, A., Nador, A., Koroknai, B., Pap, N., Toth, T., Worum, G., 2015. Evolution of the Pannonian basin and its geothermal resources. Geothermics 53, 328–352. https://doi.org/10.1016/j.geothermics.2014.07.009.

Huang, Z., Zhao, D., Wang, L., 2015. P wave tomography and anisotropy beneath Southeast Asia: Insight into mantle dynamics. J. Geophys. Res. Solid Earth 120, 5154–5174. https://doi.org/10.1002/2015JB012098.

Hubbert, M.K., 1937. Theory of scale models as applied to the study of geologic structures. Bulletin of the Geological Society of America 48 (10), 1459–1520.

Jagoutz, O., Royden, L., Holt, A.F., Becker, T.W., 2015. Anomalously fast convergence of India and Eurasia caused by double subduction. Nat. Geosci. 8, 475–478. https://doi.org/10.1038/ngeo2418.

Jarvis, A., Reuter, H.I., Nelson, A., Guevara, E., 2017. Hole-Filled SRTM for the Globe Version 4, Available from the CGIAR-CSI SRTM 90m Database (http://srtm.csi.cgiar.org). [WWW Document]. CGIAR-CSI. URL https://cgiarcsi.community/data/srtm-90m-digital-elevation-database-v4-1/ (accessed 9.18.20).

Ji, Y., Yoshioka, S., Manea, V.C., Manea, M., 2017. Seismogenesis of dual subduction beneath Kanto, Central Japan controlled by fluid release. Sci. Rep. 7, 16864. https://doi.org/10.1038/s41598-017-16818-z.

Karlsen, K.S., Domeier, M., Gaina, C., Conrad, C.P., 2020. A tracer-based algorithm for automatic generation of seafloor age grids from plate tectonic reconstructions. Comput. Geosci. 104508. https://doi.org/10.1016/j.cageo.2020.104508.

King, S.D., Hager, B.H., 1990. The relationship between plate velocity and trench viscosity in Newtonian and power-law subduction calculations. Geophys. Res. Lett. 17, 2409–2412. https://doi.org/10.1029/GL017i013p02409.

Király, Á., Capitanio, F.A., Funiciello, F., Faccenna, C., 2016. Subduction zone interaction: Controls on arcuate belts. Geology 44, 715–718. https://doi.org/10.1130/G37912.1.

Király, Á., Faccenna, C., Funiciello, F., 2018a. Subduction zones interaction around the Adria microplate and the origin of the Apenninic arc. Tectonics 37. https://doi.org/10.1029/2018TC005211.

Király, Á., Holt, A.F., Funiciello, F., Faccenna, C., Capitanio, F.A., 2018b. Modeling slab-slab interactions: dynamics of outward dipping double-sided subduction systems. Geochem. Geophys. Geosyst. 19, 693–714. https://doi.org/10.1002/2017GC007199.

Király, Á., Funiciello, F., Capitanio, F.A., Faccenna, C., 2020a. Dynamic interactions around subduction zones - research data on Central-Mediterranean analog models. GFZ Data Serv. https://doi.org/10.5880/fidgeo.2020.038.

Király, Á., Portner, D.E., Haynie, K.L., Chilson-Parks, B.H., Ghosh, T., Jadamec, M., Makushkina, A., Manga, M., Moresi, L., O'Farrell, K.A., 2020b. The effect of slab gaps on subduction dynamics and mantle upwelling. Tectonophysics 785, 228458. https://doi.org/10.1016/j.tecto.2020.228458.

Lallemand, S., Font, Y., Bijwaard, H., Kao, H., 2001. New insights on 3-D plates interaction near Taiwan from tomography and tectonic implications. Tectonophysics 335, 229–253. https://doi.org/10.1016/S0040-1951(01)00071-3.

Lamb, S., 2011. Cenozoic tectonic evolution of the New Zealand plate-boundary zone: a paleomagnetic perspective. Tectonophysics 509, 135–164. https://doi.org/10.1016/j.tecto.2011.06.005.

Liao, J., Gerya, T., Thielmann, M., Webb, A.A.G., Kufner, S.-K., Yin, A., 2017. 3D geodynamic models for the development of opposing continental subduction zones: the Hindu Kush–Pamir example. Earth Planet. Sci. Lett. 480, 133–146. https://doi.org/10.1016/j.epsl.2017.10.005.

Lippitsch, R., Kissling, E., Ansorge, J., 2003. Upper Mantle Structure beneath the Alpine Orogene from high-resolution teleseismic tomography. J. Geophys. Res. 108, 1–15. https://doi.org/10.1029/2002JB002016.

Lucente, F.P., Speranza, F., 2001. Belt bending driven by deep processes: geophysical evidences from the northern Apennines (Italy). Tectonophysics 337, 51–62.

Luth, S.W., Willingshofer, E., Sokoutis, D., Cloetingh, S., 2013. Does subduction polarity changes below the Alps? Inferences from analogue modelling. Tectonophysics 582, 140–161. https://doi.org/10.1016/j.tecto.2012.09.028.

Lyu, T., Zhu, Z., Wu, B., 2019. Subducting slab morphology and mantle transition zone upwelling in double-slab subduction models with inward-dipping directions. Geophys. J. Int. 218, 2089–2105. https://doi.org/10.1093/gji/ggz268.

Maffione, M., Speranza, F., Faccenna, C., Cascella, A., Vignaroli, G., Sagnotti, L., 2008. A synchronous Alpine and Corsica-Sardinia rotation. J. Geophys. Res. Solid Earth 113, 1–25. https://doi.org/10.1029/2007JB005214.

Magni, V., Király, Á., 2019. Delamination, in: Reference Module in Earth Systems and Environmental Sciences. Elsevier. https://doi.org/10.1016/B978-0-12-409548-9.09515-4. B9780124095489096000.

Malinverno, A., Ryan, W.B.F., 1986. Extension in the Tyrrhenian Sea and shortening in the Apennines as result of arc migration driven by sinking of the lithosphere. Tectonics 5, 227–245. https://doi.org/10.1029/TC005i002p00227.

Margheriti, L., Lucente, F.P., Pondrelli, S., 2003. SKS splitting measurements in the Apenninic-Tyrrhenian domain (Italy) and their relation with lithospheric subduction and mantle convection. J. Geophys. Res. Solid Earth 108. https://doi.org/10.1029/2002JB001793.

Margheriti, L., Lucente, F.P., Park, J., Pondrelli, S., Levin, V., Steckler, M.S., Baccheschi, P., Salimbeni, S., 2014. Large-scale coherent anisotropy of upper mantle beneath the Italian peninsula comparing quasi-Love waves and SKS splitting. J. Geodyn. 82, 26–38. https://doi.org/10.1016/j.jog.2014.07.007.

Martinod, J., Funiciello, F., Faccenna, C., Labanieh, S., Regard, V., 2005. Dynamical effects of subducting ridges: insights from 3-D laboratory models. Geophys. J. Int. 163, 1137–1150. https://doi.org/10.1111/j.1365-246X.2005.02797.x.

Matthews, K.J., Maloney, K.T., Zahirovic, S., Williams, S.E., Seton, M., Müller, R.D., 2016. Global plate boundary evolution and kinematics since the late Paleozoic. Glob. Planet. Chang. 146, 226–250. https://doi.org/10.1016/j.gloplacha.2016.10.002.

McCarthy, A., Chelle-Michou, C., Müntener, O., Arculus, R., Blundy, J., 2018. Subduction initiation without magmatism: The case of the missing Alpine magmatic arc. In: Geological Society of America | Geology, 46. https://doi.org/10.1130/G45366.1.

Mishin, Y.A., Gerya, T.V., Burg, J.-P., Connolly, J.A.D., 2008. Dynamics of double subduction: Numerical modeling. In: Physics of the Earth and Planetary Interiors, Recent Advances in Computational Geodynamics: Theory, Numerics and Applications, 171, pp. 280–295. https://doi.org/10.1016/j.pepi.2008.06.012.

Molli, G., Malavieille, J., 2011. Orogenic processes and the Corsica/Apennines geodynamic evolution: insights from Taiwan. Int. J. Earth Sci. 100, 1207–1224. https://doi.org/10.1007/s00531-010-0598-y.

Müller, R.D., Sdrolias, M., Gaina, C., Roest, W.R., 2008. Age, spreading rates, and spreading asymmetry of the world's ocean crust. Geochem. Geophys. Geosyst. 9 https://doi.org/10.1029/2007GC001743 n/a-n/a.

Peral, M., Király, Á., Zlotnik, S., Funiciello, F., Fernàndez, M., Faccenna, C., Vergés, J., 2018. Opposite subduction polarity in adjacent plate segments. Tectonics 1–18. https://doi.org/10.1029/2017TC004896.

Peral, M., Ruh, J., Zlotnik, S., Funiciello, F., Fernàndez, M., Vergés, J., Gerya, T., 2020. Analog and numerical experiments of double subduction systems with opposite polarity in adjacent segments. Geochem. Geophys. Geosyst. 21 https://doi.org/10.1029/2020GC009035 e2020GC009035.

Piromallo, C., Morelli, A., 2003. P wave tomography of the mantle under the Alpine-Mediterranean area. J. Geophys. Res. 108, 1–23. https://doi.org/10.1029/2002JB001757.

Pusok, A.E., Stegman, D.R., 2019. Formation and stability of same-dip double subduction systems. J. Geophys. Res. Solid Earth 124, 7387–7412. https://doi.org/10.1029/2018JB017027.

Royden, L., Faccenna, C., 2018. Subduction orogeny and the Late Cenozoic evolution of the Mediterranean Arcs. Annu. Rev. Earth Planet. Sci. 46, 261–289. https://doi.org/10.1146/annurev-earth-060115.

Salimbeni, S., Malusà, M.G., Zhao, L., Guillot, S., Pondrelli, S., Margheriti, L., Paul, A., Solarino, S., Aubert, C., Dumont, T., Schwartz, S., Wang, Q., Xu, X., Zheng, T., Zhu, R., 2018. Active and fossil mantle flows in the western Alpine region unravelled by seismic anisotropy analysis and high-resolution P wave tomography. Tectonophysics 731–732, 35–47. https://doi.org/10.1016/j.tecto.2018.03.002.

San Jose, M., Caves Rugenstein, J.K., Cosentino, D., Faccenna, C., Fellin, M.G., Ghinassi, M., Martini, I., 2020. Stable isotope evidence for rapid uplift of the central Apennines since the late Pliocene. Earth Planet. Sci. Lett. 544, 116376. https://doi.org/10.1016/j.epsl.2020.116376.

Schefer, S., Cvetkovic, V., Fügenschuh, B., Kounov, A., Ovtcharova, M., Schaltegger, U., Schmid, S.M., Cvetković, V., Fügenschuh, B., Kounov, A., Ovtcharova, M., Schaltegger, U., Schmid, S.M., 2011. Cenozoic granitoids in the Dinarides of southern Serbia: Age of intrusion, isotope geochemistry, exhumation history and significance for the geodynamic evolution of the Balkan Peninsula. Int. J. Earth Sci. 100, 1181–1206. https://doi.org/10.1007/s00531-010-0599-x.

Serpelloni, E., Faccenna, C., Spada, G., Dong, D., Williams, S.D.P., 2013. Vertical GPS ground motion rates in the Euro-Mediterranean region: new evidence of velocity gradients at different spatial scales along the Nubia-Eurasia plate boundary. J. Geophys. Res. Solid Earth 118, 6003–6024. https://doi.org/10.1002/2013JB010102.

Soesoo, A., Bons, P.D., Gray, D.R., Foster, D.A., 1997. Divergent double subduction: tectonic and petrologic consequences. Geology 25, 755–758. https://doi.org/10.1130/0091-7613(1997)025<0755:DDSTAP>2.3.CO;2.

Speranza, F., Sagnotti, L., Mattei, M., 1997. Tectonics of the Umbria-Marche-Romagna Arc (central northern Apennines, Italy): new paleomagnetic constrain. J. Geophis. Res. 102, 3153–3166.

Stampfli, G.M., 2000. Tethyan oceans. Geol. Soc. Lond., Spec. Publ. 173, 1–23. https://doi.org/10.1144/GSL.SP.2000.173.01.01.

Sternai, P., Sue, C., Husson, L., Serpelloni, E., Becker, T.W., Willett, S.D., Faccenna, C., Di Giulio, A., Spada, G., Jolivet, L., Valla, P., Petit, C., Nocquet, J.-M., Walpersdorf, A., Castelltort, S., 2019. Present-day uplift of the European Alps: evaluating mechanisms and models of their relative contributions. Earth Sci. Rev. 190, 589–604. https://doi.org/10.1016/j.earscirev.2019.01.005.

Strak, V., Schellart, W.P., 2014. Evolution of 3-D subduction-induced mantle flow around lateral slab edges in analogue models of free subduction analysed by stereoscopic particle image velocimetry technique. Earth Planet. Sci. Lett. 403, 368–379. https://doi.org/10.1016/j.epsl.2014.07.007.

Subašić, S., Prevolnik, S., Herak, D., Herak, M., 2017. Observations of SKS splitting beneath the Central and Southern External Dinarides in the Adria-Eurasia convergence zone. Tectonophysics 705, 93–100. https://doi.org/10.1016/j.tecto.2017.03.027.

Šumanovac, F., Markušić, S., Engelsfeld, T., Jurković, K., Orešković, J., 2017. Shallow and deep lithosphere slabs beneath the Dinarides from teleseismic tomography as the result of the Adriatic lithosphere downwelling. Tectonophysics 712–713, 523–541. https://doi.org/10.1016/j.tecto.2017.06.018.

Sun, W., Zhao, L., Malusà, M.G., Guillot, S., Fu, L.-Y., 2019. 3-D Pn tomography reveals continental subduction at the boundaries of the Adriatic microplate in the absence of a precursor oceanic slab. Earth Planet. Sci. Lett. 510, 131–141. https://doi.org/10.1016/j.epsl.2019.01.012.

Thielicke, W., Stamhuis, E.J., 2014. PIVlab - towards user-FRIENDLY, affordable and accurate digital particle image velocimetry in MATLAB. J. Open Res. Softw. 2, e30. https://doi.org/10.5334/jors.bl.

Tichelaar, B.W., Ruff, L.J., 1993. Depth of seismic coupling along subduction zones. J. Geophys. Res. Solid Earth 98, 2017–2037. https://doi.org/10.1029/92JB02045.

Toljić, M., Matenco, L., Stojadinović, U., Willingshofer, E., Ljubović-Obradović, D., 2018. Understanding fossil fore-arc basins: Inferences from the Cretaceous Adria-Europe convergence in the NE Dinarides. In: Global and Planetary Change, From the deep Earth to the Surface, 171, pp. 167–184. https://doi.org/10.1016/j.gloplacha.2018.01.018.

Ustaszewski, K., Schmid, S.M., Lugović, B., Schuster, R., Schaltegger, U., Bernoulli, D., Hottinger, L., Kounov, A., Fügenschuh, B., Schefer, S., 2009. Late Cretaceous intra-oceanic magmatism in the internal Dinarides (northern Bosnia and Herzegovina): Implications for the collision of the Adriatic and European plates. In: Lithos, Ophiolites and Related Geology of the Balkan Region, 108, pp. 106–125. https://doi.org/10.1016/j.lithos.2008.09.010.

van Benthem, S., Govers, R., Spakman, W., Wortel, R., 2013. Tectonic evolution and mantle structure of the Caribbean. J. Geophys. Res. Solid Earth 118, 3019–3036. https://doi.org/10.1002/jgrb.50235.

van der Meer, D.G., van Hinsbergen, D.J.J., Spakman, W., 2018. Atlas of the underworld: slab remnants in the mantle, their sinking history, and a new outlook on lower mantle viscosity. Tectonophysics 723, 309–448. https://doi.org/10.1016/j.tecto.2017.10.004.

Van der Voo, R., Spakman, W., Bijwaard, H., 1999. Tethyan subducted slabs under India. Earth Planet. Sci. Lett. 171, 7–20. https://doi.org/10.1016/S0012-821X(99)00131-4.

van Hinsbergen, D.J.J., Torsvik, T.H., Schmid, S.M., Maţenco, L.C., Maffione, M., Vissers, R.L.M., Gürer, D., Spakman, W., 2020. Orogenic architecture of the Mediterranean region and kinematic reconstruction of its tectonic evolution since the Triassic. Gondwana Res. 81, 79–229. https://doi.org/10.1016/j.gr.2019.07.009.

Vignaroli, G., Faccenna, C., Jolivet, L., Piromallo, C., Rossetti, F., 2008. Subduction polarity reversal at the junction between the Western Alps and the Northern Apennines, Italy. Tectonophysics 450, 34–50. https://doi.org/10.1016/j.tecto.2008.10.01.

von Blackenburg, F., Davies, J.H., 1995. Slab breakoff: a model for syncollisional magmatism and tectonics in the Alps. Tectonics 14, 120–131.

Wei, W., Xu, J., Zhao, D., Shi, Y., 2012. East Asia mantle tomography: New insight into plate subduction and intraplate volcanism. J. Asian Earth Sci. 60, 88–103. https://doi.org/10.1016/j.jseaes.2012.08.001.

Wortel, M.J., Spakman, W., 2000. Subduction and slab detachment in the Mediterranean-Carpathian region. Science (New York, N.Y.) 290, 1910–1917. https://doi.org/10.1126/science.290.5498.1910.

Zhang, Q., Guo, F., Zhao, L., Wu, Y., 2017. Geodynamics of divergent double subduction: 3-D numerical modeling of a Cenozoic example in the Molucca Sea region, Indonesia. J. Geophys. Res. Solid Earth. https://doi.org/10.1002/2017JB013991.

Zhao, L., Paul, A., Malusà, M.G., Xu, X., Zheng, T., Solarino, S., Guillot, S., Schwartz, S., Dumont, T., Salimbeni, S., Aubert, C., Pondrelli, S., Wang, Q., Zhu, R., 2016. Continuity of the Alpine slab unraveled by high-resolution P wave tomography. J. Geophys. Res. Solid Earth 121, 8720–8737. https://doi.org/10.1002/2016JB013310.

Zhong, S., Gurnis, M., 1994. Controls on trench topography from dynamic models of subducted slabs. J. Geophys. Res. Solid Earth 99, 15683–15695. https://doi.org/10.1029/94JB00809.

Zhu, D.-C., Li, S.-M., Cawood, P.A., Wang, Q., Zhao, Z.-D., Liu, S.-A., Wang, L.-Q., 2016. Assembly of the Lhasa and Qiangtang terranes in central Tibet by divergent double subduction. In: Lithos, Recent Advances on the Tectonic and Magmatic Evolution of the Greater Tibetan Plateau: A Special Issue in Honor of Prof. Guitang Pan, 245, pp. 7–17. https://doi.org/10.1016/j.lithos.2015.06.023.